Journal of Fluorescence
https://doi.org/10.1007/s10895-023-03564-x

RESEARCH

Interactions Between Silver Nanoparticles and Culture Medium Biomolecules with Dose and Time Dependencies

Cristofher Victor Vivas[1] · Evandro Luiz Duarte[1] · Yan Borges Barreto[1] · Cristiano Luis Pinto deOliveira[1] · Sergio Hiroshi Toma[2] · Jonnatan Julival Santos[2] · Koiti Araki[2] · Adriano Mesquita Alencar[1] · Antonio Carlos Bloise[1]

Received: 24 November 2023 / Accepted: 20 December 2023

Abstract

The interaction between silver nanoparticles (AgNPs) and molecules producing coronas plays a key role in cytotoxicity mechanisms. Once adsorbed coronas determine the destiny of nanomaterials in vivo, their effective deployment in the biomedical field requires a comprehensive understanding of the dynamic interactions of biomolecules with nanoparticles. In this work, we characterized 40 nm AgNPs in three different nutritional cell media at different molar concentrations and incubation times to study the binding mechanism of molecules on surface nanoparticles. In addition, their cytotoxic effects have been studied in three cell lineages used as tissue regeneration models: FN1, HUV-EC-C, RAW 264.7. According to the data, when biomolecules from DMEM medium were in contact with AgNPs, agglomeration and precipitation occurred. However, FBS medium proteins indicated the formation of coronas over the nanoparticles. Nonetheless, little adsorption of molecules around the nanoparticles was observed when compared to DMEM supplemented with 10% FBS. These findings indicate that when nanoparticles and bioproteins from supplemented media interact, inorganic salts from DMEM contribute to produce large bio-coronas, the size of which varies with the concentration and time. The static quenching mechanism was shown to be responsible for the fluorescence quenching of the bioprotein aggregates on the AgNPs surface. The calculated bioprotein-nanoparticle surface binding constants were on the order of 10^5 M^{-1} at 37 °C, with hydrophobic interactions driven by enthalpy and entropy playing a role, as confirmed by thermodynamic analysis. Cytotoxicity data showed a systematic degrowth in the viable cell population as the number of nanoparticles increased and the diameter of coronas decreased. Cytotoxic intervals associated with half decrease of cell population were established for AgNPs molar concentration of 75 μM for 24 h and 50 μM for 48 h. In summary, through the cytotoxicity mechanism of bio-coronas we are able to manipulate cells' expansion rates to promote specific processes, such inflammatory mechanisms, at different time instants.

Keywords Silver nanoparticles AgNPs · Dulbecco's Modified Eagle's Medium DMEM · Fetal bovine serum FBS · Bio-coronas · Cytotoxicity · Cells

Introduction

Due to their biological functionality and antimicrobial properties, silver nanoparticles (AgNPs) are the most commercialized nanomaterials, thus gaining great scientific interest and applications in the biomedical field [1]. Despite their beneficial properties, there is an ongoing debate regarding the toxicological effects of AgNPs and serious toxicological effects have been reported in vitro and in vivo model systems [2, 3]. Current research results indicate that the inherent cytotoxicity of AgNPs might be a useful tool to modulate metabolic cell functions during wound healing, thus restricting the formation of pathological scars and other associated disorders [4–6]. Different cytotoxic effects and biochemical events can be induced depending on the biodistribution and cellular uptake of AgNPs [7, 8]. Therefore, developing new approaches that promote more appropriate or easier internalization of AgNPs in cells is important.

✉ Cristofher Victor Vivas
vivas@if.usp.br

✉ Antonio Carlos Bloise
acbloise@usp.br

[1] Instituto de Fisica, Universidade de Sao Paulo, Sao Paulo, Brazil

[2] Instituto de Quimica, Universidade de Sao Paulo, Sao Paulo, Brazil

Published online: 06 January 2024

When AgNPs are in contact with proteins or biomolecules, they rapidly adsorb onto their nanoparticle surfaces [9], forming a hard biomolecular corona [10, 11]. The composition of the corona depends upon a series of competitive processes driven by both thermodynamic and kinetic factors [12]. This biological nanoparticle entity acquires a new identity, which has a specific affinity for its receptor protein on the cell membrane [13]. In fact, drug delivery strategies have been developed in recent years as a consequence of this new identity [14]. Despite this significant innovation, studies have shown that biomolecule adsorption can alter the characteristics of AgNPs, such as size, shape, and agglomeration state [15]. Accordingly, changes in cellular uptake, intracellular localization, tumor accumulation, and toxicity have been reported [16].

Dulbecco's Modified Eagle's Medium (DMEM) supplemented with fetal bovine serum (FBS) is a basal culture medium that is widely used to support the growth, proliferation, and differentiation of many different cell lineages [17]. Albumin is the primary protein component of the fetal bovine serum medium [14], in addition to globulins and hemoglobin, which represent 35% of the total composition. AgNPs are widely recognized for their ability to form a protein corona structure with those proteins [18]. The binding mechanism has been extensively characterized, showing spontaneous hydrophobic forces [19] van der Waals interactions, and entropy-driven binding [20]. Regarding DMEM, the main components of this other physiological medium are amino acids, organic salts, and vitamins. The interactions between these biomolecules and nanoparticles are not fully understood; however, a recent study showed that the adsorption of components from the basal culture medium (biomolecules + proteins) onto the surface of AgNPs forms corona structures [21]. In another work, it was highlighted that incubation time is an important parameter for corona concentration and composition [22, 23]. They showed that increasing the concentration of FBS during the formation of the protein corona, led to the increasing of corona protein concentration as a function of both the incubation time and concentration [23]. It was seen in another study, when gold NPs were incubated with pooled plasma samples at room 37 °C the total amount of protein decreased with time from 5 to 60 min [24]. It is also known that the biological response to nanoparticle cytotoxicity can be either enhanced or diminished by the size of the corona, concentration, and incubation time [25, 26]. Therefore, developing interaction models between AgNPs and DMEM-biomolecules and AgNPs and FBS proteins is important for understanding the composition and dynamic formation of the corona complex bioprotein/AgNP when the nanoparticles are in contact with the basal culture medium.

In this work, the morpho-electrical properties of AgNPs in three different nutritional physiological environments, DMEM, FBS, and DMEM + 10% FBS, were evaluated at different concentrations and incubation times using dynamic light scattering (DLS), zeta potential (ZP), small-angle X-ray scattering (SAXS), and UV–vis absorption spectroscopy. In the system composed by the AgNPs diluted in DMEM + 10% FBS, steady-state and time-resolved fluorescence measurements were also used to understand and quantify the binding adsorption process of bioproteins to AgNPs surface. Finally, in order to evaluate the cytotoxic effect of the bioprotein/AgNP complex on cellular growth of human dermal microvascular endothelial cells (HUV-EC-C), human fibroblast cells (FN1), and murine macrophages (RAW 264.7) [5, 6], we critically examined and compared the responses of all these cell lineages after exposure to the bioprotein corona. In summary, we demonstrated the ability of FBS proteins and DMEM-biomolecules to tangle around a hard silver nanoparticle core, forming a 3D complex bio-structure, as well as the effect of this complex on cellular viability. The uptake of AgNPs triggering all cytotoxicity effects was shown to be strongly influenced by the shape and density of biomolecules bound on the nanoparticles' surface.

Materials and Methods

Materials

Dulbecco's Modified Eagle's Medium high glucose (pure DMEM, Gibco®) with 17.0 g L^{-1} (200 mM) of biomolecules and inactivated/sterile Fetal Bovine Serum (pure FBS, Gibco®) with 70.0 g L^{-1} (785.4 μM) of proteins were obtained from Sigma Aldrich (St. Louis, Missouri, United States). The supplemented cell culture medium was prepared by diluting 50 mL of FBS in 450 mL of pure DMEM, obtaining a solution named as basal supplemented culture medium composed of 10% (v/v) FBS in pure DMEM. All the reagents listed above were of analytical grade and were used without further purification.

Silver Nanoparticles Synthesis

Stable dispersions of spherical-shaped AgNPs with average diameter of 40.0 ± 0.6 nm measured by DLS, with 27.3 mg L^{-1} (250.3 μM) of elemental silver as confirmed by ICP-OES, were synthesized by the Turkevich method [27], by refluxing a silver salt with citric acid as a reducing and stabilizing agent to the nanoparticles in aqueous solution. Briefly, 4.25 mg of silver nitrate (anhydrous ≥ 99.999% trace metals base, Sigma-Aldrich®, St. Louis, USA) was solubilized in 100 mL of ultrapure water (18 M Ω.cm) and heated. Then, 1 mL of a 0.5 M citric acid solution (anhydrous, ≥ 99.5%, Sigma-Aldrich®) was added into the boiling silver solution and kept under stirring for 5 min.

The reaction medium was cooled to room temperature and filtered through a 0.2 μm (Corning®, New York, USA) sterile cellulose membrane syringe filter resulting in stable AgNP dispersions. The concentration of elemental silver was determined by dissolving the AgNPs with concentrated nitric acid, diluting with ultrapure water and analyzing by ICP-OES. The final concentration was determined based on a calibration curve prepared using a certified silver analytical standard (TraceCERT®, Sigma-Aldrich) diluted in aqueous 2% nitric acid. Table 1 summarizes the sample scheme of incubation and characterization.

Corona Formation Study

The samples used to study corona formation (seen Supplementary Table 1 in the Supplementary Information section) were prepared by diluting the stock dispersion of AgNPs (250.3 µM of Ag) in three different physiological environments: (i) DMEM + 10% (v/v) ultrapure water (DMEM, 180.0 mM of biomolecules), (ii) ultrapure water + 10% (v/v) FBS (FBS, 78.5 μM of proteins), and (iii) DMEM + 10% (v/v) FBS (180.1 mM of bioproteins). It is important to note here that the terminology "bioproteins" given to the supplemented DMEM refers to the combination of biomolecules from DMEM with the proteins from FBS. Aliquots of these solutions were transferred into culture well plates, and incubated at 37 °C, 5% CO_2 atmosphere, for 24 and 48 h in a commercial incubator (Series II Water Jacket, Thermo Scientific, Waltham, MA, USA) to simulate the cellular environment. After incubation, the solutions were centrifuged at 14,500 rpm for 15 min [19]. The unbound fractions of DMEM biomolecules, FBS proteins, and bioproteins DMEM + FBS in the supernatant were pipetted out and the pellets were washed three times with an equal amount of ultrapure water and resuspended again in ultrapure water for the further studies. Samples were prepared in triplicate and used for further characterization. Table 1 summarizes the sample incubation schemes.

Dynamic Light Scattering (DLS)

Size distribution of nanoparticles in aqueous suspension was determined by DLS using a Malvern Zetasizer Nano-ZS90 (Worcestershire, UK) equipment. Measurements were performed in a triplicates scheme (Table 1). For each sample, we performed three measurements, each one with 20 runs, a fixed detector angle of 90°, using a 532 nm laser, and a quartz cuvette with 10.0 mm of optical path. The temperature was kept at 37 °C to simulate the cellular environment. The volume of sample used in the measurements was kept constant at 1 mL for all investigated samples. Due to ultrapure water being used as the main solvent that composes the samples, silver nanoparticles and culture media, it adopted its viscosity, 0.6864 cP, and refractive index, 1.33, as inputs to the DLS system to acquire the data.

Transmission Electron Microscopy (TEM)

TEM experiments for stock silver nanoparticles were performed using a JEOL field emission microscope, model JEM 2100 FEG-TEM, equipped with a field emission gun (FEG) at an acceleration voltage of 200 kV. Measurements were performed in a triplicates scheme.

Zeta-potential (ZP)

Surface charge data of nanoparticles from ZP were obtained using the same Malvern Zetasizer Nano-ZS90 equipment used in DLS measurements, in a triplicate scheme (Table 1). For each sample, we performed three measurements, each one with 20 sub-runs, at 37 °C, using a 532 nm laser, fixed detector angle of 17°, and folded capillary cell using the same samples of AgNPs dispersions used in the DLS measurements. For these measurements, the pH of AgNPs stock was 7.70 ± 0.40, whereas for the FBS, DMEM and DMEM + 10% FBS were, respectively, 8.10 ± 0.03, 7.30 ± 0.05, and 8.59 ± 0.01. They were obtained taking four reads in the time, 5, 7.5, 10, and 15 min after inserted pH-probe, and using 1 mL for each sample.

Table 1 Strategy used for preparation of the samples *per* study, indicating the doses, incubation times, and the number of replicates used in each experiment

Experiment	*AgNPs dose (µM)*	*Incubation time (h)*	*Replicates per dose / measurements*	*Total wells-cultivated*
DLS	0/25/50/75/100/250.3	24/48	3/3	36
ZP	0/25/50/75/100/250.3	24/48	3/3	36
UV–vis	0/25/50/75/100/250.3	24/48	3/3	36
SAXS	0/25/50/75/100/250.3	24/48	3/3	36
SSF	0/25/50/75/100	24/48	3/3	30
TRF	0/25/50/75/100	24/48	3/3	30
Cell proliferation	0/25/50/75/100	24/48	4/0	40

Small-angle X-ray Scattering (SAXS)

Small angle X-ray scattering data collection was performed with Xenocs XEUSS™ version 2.0 equipment. The scattering intensity is expressed as a function of the reciprocal space momentum transfer modulus, $q = 4\ \pi \sin(\theta/\lambda)$, where $2\ \theta$ is the scattering angle and λ the radiation wavelength. Samples were placed in a quartz capillary (1.5 mm, 0.4 mL) and measurements were performed at 37 °C. The radiation was generated by a GENIX3D™ X-ray source (Cu K α edge, λ=1.54 Å) with the beam focused by FOX2D™ optics. The 2D data were collected at the EMUSAXS Multiuser SAXS facility, where the scattering data were normalized to absolute scale using water as the primary standard. The experimental SAXS data were modeled using the Indirect Fourier Transformation method—IFT [28] in a slightly different implementation [29]. From the IFT method the pair distance distribution function $p(r)$ is obtained and can provide a direct indication of the average particle shape and size [30].

Ultraviolet–visible Absorption Spectroscopy (UV–vis)

Optical absorption spectra were recorded with a Varian Cary 50 UV–Vis spectrophotometer (Santa Clara, CA). Samples were placed in a quartz cuvette (0.4 × 1.0 cm, 0.5 mL), with the absorption optical pathway of 0.4 cm. The temperature was controlled at 37 °C with a Carry Peltier thermostat and the measurements were carried out in the 200 to 800 nm range.

Fluorescence Study of Bioprotein-AgNPs Corona

Among all the biological molecules present in the culture media, we decided to investigate the changes in the fluorescence intensity of tryptophan from DMEM + 10% FBS in the absence and presence of silver. For this, a set of samples was prepared by diluting the concentrated stock dispersion of AgNPs (250.3 µM) to 25, 50, 75, and 100 µM in DMEM + 10% FBS. The samples were prepared maintaining constant the DMEM + 10% FBS amount (100.0 mM bioprotein) in 25 – 100 µM of silver NPs. The volumes of the AgNP stock were adjusted in ultrapure water to obtain the silver molar concentrations in this study. Samples, including DMEM + 10% FBS in absence of silver, were transferred into culture well plates for steady-state and time-resolved fluorescence assays. These plates were then transferred to an incubator and left for 24 and 48 h at 37 °C to simulate the cellular environment. As usual, the triplicate scheme of sample preparation was used and two identical sets of samples were incubated for 24 and 48 h, as summarized in Table 1.

Steady-state Fluorescence Spectroscopy (SSF)

A Varian Cary Eclipse spectrometer was used for Tryptophan steady-state fluorescence intensity measurement as a function of silver nanoparticle concentration. Samples were placed in quartz cuvettes (0.4 cm × 1.0 cm, 0.5 mL), with the incident beam parallel to the 0.4 cm pathway. The static fluorescence experiments were performed with an excitation wavelength of 280 nm, with slits for excitation and emission adjusted to 5 nm. The temperature was kept at 37 °C to simulate the cellular environment. The inner filter correction [31] was applied to all fluorescent emission spectra by using the following equation.

$$F_{corr}(\lambda) = F_{obs}(\lambda)10^{(A_{exc}.l+A_{emi}.l')}$$

where $F_{corr}(\lambda)$ and $F_{obs}(\lambda)$ are the corrected and observed fluorescence intensities, A_{exc} and A_{emi} are the absorbance *per* unit of pathway at the excitation and emission wavelengths. In addition, the l and l' parameters are the optical pathways in cm for excitation (0.2 cm) and for emission (0.5 cm), considering the cuvette center.

Time Resolved Fluorescence Spectroscopy (TRF)

Time-resolved fluorescence measurements were performed using time-correlated single photon counting (TCSPC). The fluorescent decay of tryptophan in the presence of silver nanoparticles was recorded at 37 °C to simulate the cellular environment. The excitation light at 280 nm is produced by a titanium-sapphire Tsunami 3950 laser (Newport Corporation, Irvine, CA,USA), pumped by a Millenia Pro model J8o solid-state laser, both from Spectra Physics. The frequency rate of pulse repetition was set to 8 MHz using a Spectra Physics 3980–25 pulse picker. The Tsunami laser was set to provide an output at 840 nm while third harmonic generator BBO crystal (GWN-23 PL Spectra Physics) was used to generate the excitation beam at 280 nm. The emission at 90° from the excitation beam and selected by a monochromator at 350 nm was detected by a refrigerated Hamamatsu R3809U photomultiplier. The FAST software supplied by Edinburgh Instruments was used to fit the data by applying an exponential decays model [31] according to the following equation.

$$F(\lambda, t) = \Sigma^{N}{}_{i=1}\alpha_i.\exp(-t/\tau_i)$$

where $F(\lambda,t)$ is the number of photons emitted at a given wavelength λ at time t, α_i is the pre-exponential factor, and τ_i the lifetime of the i^{th} component of the decay curve.

Cytotoxicity of the AgNPs/bioprotein Complex

Microvascular endothelial cells (HUV-EC-C), human fibroblast cells (FN1), and murine macrophages (RAW 264.7) were grown on 16.25 mm glass coverslips placed in two

24-well plates with a seeding density of 2×10^5 cells *per* coverslip. After 12 h, AgNP/bioprotein complexes (25, 50, 75, and 100 μM of silver) and supplemented culture medium (free of silver) were incubated with cells for 24 and 48 h, and cytotoxicity estimated as a function of the respective cell proliferation rates evaluated using a Neubauer hemocytometer (OptikLabor Görlizt, Germany). The replicated number for each sample is depicted in Table 1.

Data Processing Statistics

All statistical analyses were performed using Student's *t*-test with a confidence level of 95% ($p < 0.05$) to determine the differences in average values and results presented as mean ± standard deviation (SD). All analyses were performed using the Minitab software, version 7 for MS-Windows (Minitab Inc., institutional license, State College, PA, USA).

Results and Discussion

Characterization of AgNPs Stock, DMEM, FBS, and DMEM + 10% FBS

Stock nanoparticles incubated for 24 and 48 h with pHs of 7.70 ± 0.40 and 7.75 ± 0.30 were characterized by SAXS, DLS, ZP, and UV–vis analyses, and the results are presented in Fig. 1. As can be seen in the figure, the stock AgNPs does not exhibit substantial changes in its morpho-electrical characteristics as a function of incubation time. SAXS data analyses, summarized by $I(q)$ and $p(r)$ curves, indicated that the stock suspension is constituted by nanoparticles with spherical shape and average radius of 17.0 ± 2.0 nm (Fig. 1a and e). DLS and TEM measurements confirmed this result indicating a well-defined hydrodynamic diameter of 41.7 ± 0.8 nm and a low size polydispersity index value, PDI, estimated as 0.14 ± 0.01, suggesting monodisperse silver nanoparticles (Fig. 1b and Supplementary Fig. 1 of Supplementary Materials). The negative zeta potential of -33.6 ± 0.7 mV (Fig. 1c) is consistent with the high colloidal stability conferred by citrate as stabilizing agent. Finally, UV–vis spectrum (Fig. 1d) revealed a strong absorbance around 418 nm, which is characteristic of localized surface plasmonic resonance (LSPR) absorption [32].

The DLS data registered after 24 and 48 h of incubation (Fig. 1b and e) of ultrapure water + 10% FBS in absence of silver with pHs of 8.10 ± 0.03 and 8.23 ± 0.07 (FBS, brown lines) presented a multimodal size distribution ranging from 1 to 1300 nm. There were detected peaks around 51 and 300 nm presenting the highest intensities and two others at 5 and 1300 nm, but with much lower intensities. The peaks broadened are indicating a wider size distribution. This behavior is consistent with the high PDI value of 0.70 ± 0.40 (Fig. 1e), suggesting the formation of protein agglomerates with high polydispersity, as expected for interconnected proteins such as albumin, globulin, and hemoglobin [33]. In addition, the ZP of FBS was found to be -13.9 ± 2.6 mV after 24 and 48 h suggesting its negatively charged surface [15]. Similar DLS and ZP results have been reported by Dąbkowska et al. and Gunnarsson et al. for the 10% FBS in PBS and RMID media, indicating that in the dispersion there are a large variety of proteins with different sizes and charges [34, 35]. The UV–vis spectra after 24 and 48 h of incubation exhibited a strong absorbance at around 280 nm, characteristic of tryptophan present in the proteins [36], and another with a much lower intensity at 414 nm that can be assigned to the Soret band of iron(II) protoporphyrin IX moiety in hemoglobin [37].

In contrast to FBS, DMEM + 10% ultrapure water in absence of silver (pHs of 7.30 ± 0.05 and 7.10 ± 0.08 for 24 and 48 h respectively) exhibited a peak around 0.31 ± 0.03 nm (DMEM, Fig. 1b, dark yellow line) in the DLS histogram after 24 and 48 h of incubation, and no surface potential could be measured. These results indicate that the amino acids, organic salts, and vitamin molecules present in DMEM do not form agglomerates and are fully dissolved in ultrapure water. The respective UV–Vis absorption spectra (Fig. 1d) showed an absorption band at 280 nm ascribed to tryptophan, and at 415 and 560 nm characteristic of the phenol red solution used as a pH indicator [38].

DMEM supplemented with 10% FBS in absence of silver (pHs of 8.59 ± 0.01 and 8.37 ± 0.05 for 24 and 48 h respectively), DMEM + 10% FBS (pink lines), showed a dynamic interaction between biomolecules from DMEM and proteins from FBS to form bioprotein agglomerates, which changed their morpho-electrical characteristics over time. The results obtained from SAXS, summarized by the SAXS curves, $I(q)$, and the pair distances distribution functions, $p(r)$, in Fig. 1a, indicated that bioprotein agglomerates presented a temporal evolution in their shape and size, with average radius shifting from 3.0 ± 1.0 nm after 24 h to 5.0 ± 0.5 and 12.0 ± 1.0 nm after 48 h. DLS results confirmed this behavior, showing a tendency of increasing average diameters of the multimodal size distribution of albumin/globulin/hemoglobin protein agglomerates for FBS diluted in ultrapure water (brown line, Fig. 1b) as for FBS diluted in DMEM (pink line, Fig. 1b). For 24 h, the histogram showed the highest intensity peaks at 10 and 56 nm, and another at 365 nm with much lower intensity. Nevertheless, the average diameters of the highest intensity peaks increased to 14 and 60 nm and negative ZP decreased to -7 mV (Fig. 1c and table of Fig. 1e), suggesting the formation of less colloidally stable and more polydisperse bioprotein agglomerates after 48 h of incubation, as confirmed by the calculated PDI value to 0.90 ± 0.02. When compared with the ZP results of FBS diluted in ultrapure

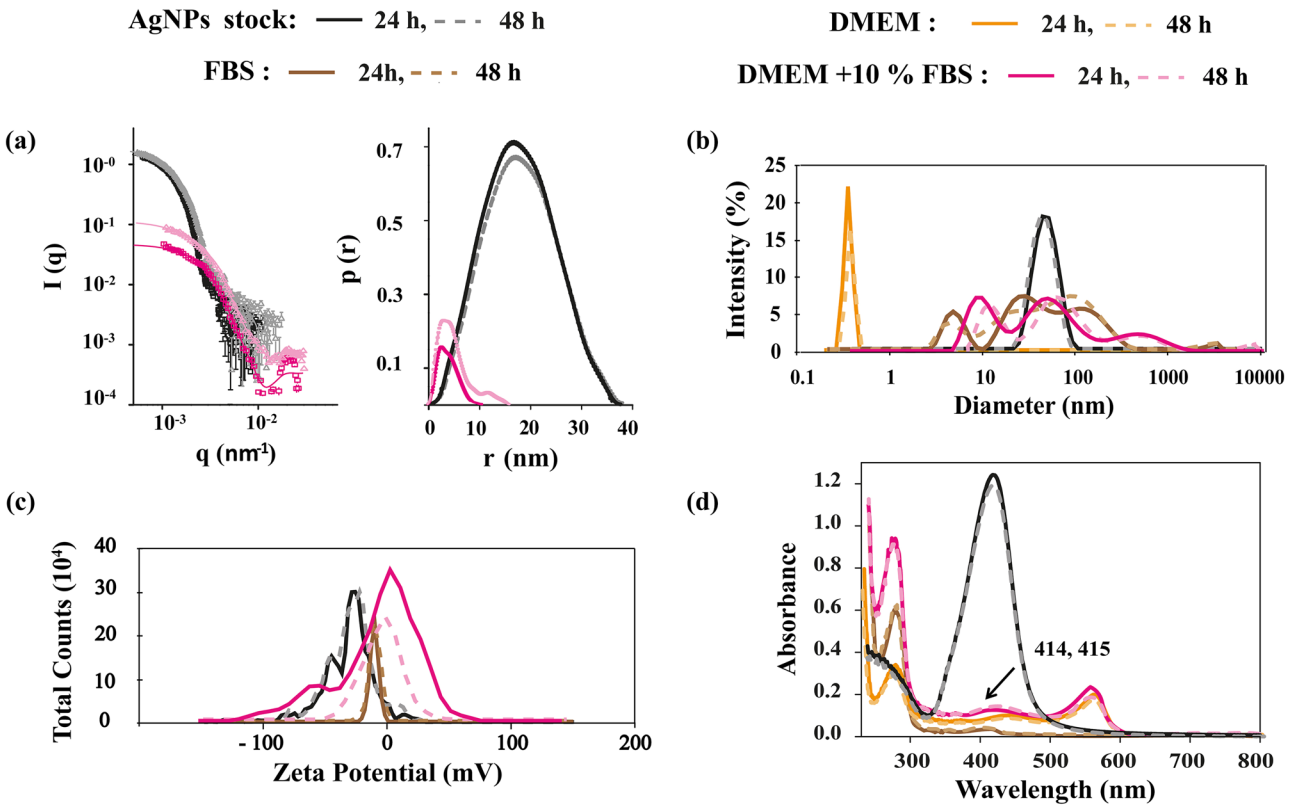

(e)

Sample	Incubation time					
	24 h					
	SAXS r (nm)	DLS d (nm)	PDI	Zeta potential ζ (mV)	UV-vis λ_{max} (nm)	pH
AgNPs stock	17.0 ± 2.0	41.7 ± 0.8	0.14 ± 0.01	- 33.6 ± 0.7	418 ± 2	7.70 ± 0.40
FBS		M.D.	0.70 ± 0.40	- 13.9 ± 2.6	280 ± 1	8.10 ± 0.03
DMEM		0.31 ± 0.03	0.10 ± 0.01	n.i.	280 ± 2 ; 560 ± 1	7.30 ± 0.05
DMEM + 10% FBS	5.0 ± 0.5	M.D.	0.90 ± 0.02	- 6.4 ± 2.8	280 ± 1 ; 560 ± 3	8.59 ± 0.01
	48 h					
AgNPs stock	18.0 ± 1.0	41.0 ± 0.5	0.10 ± 0.02	- 33.3 ± 0.3	420 ± 3	7.75 ± 0.30
FBS		M.D.	0.80 ± 0.10	- 13.3 ± 1.3	280 ± 2	8.23 ± 0.07
DMEM		0.34 ± 0.08	0.10 ± 0.01	n.i.	280 ± 1 ; 560 ± 1	7.10 ± 0.08
DMEM + 10% FBS	12.0 ± 0.5	M.D.	0.96 ± 0.03	- 7.1 ± 0.3	280 ± 2 ; 560 ± 2	8.37 ± 0.05

Fig. 1 Representative plots for AgNPs stock and three different nutrient cell media in the absence of silver nanoparticles. **a** experimental SAXS curves (symbols) and model fits (solid lines), on the left, and functions of pairwise distance distribution on the right; **b** diameter distribution obtained by DLS; **c** surface potential curves obtained from ZP measurements; **d** optical absorption spectra acquired by UV–vis measurements; **e** summary of the main results obtained from the characterization of the samples. Key: solid lines for samples incubated at 24 h and dashed lines for samples incubated at 48 h; plots using black colors for AgNPs stock; brown for FBS; dark yellow for DMEM; and pink for DMEM + 10% FBS. Abbreviations: PDI, polydispersity index; M. D. and n. i. indicate multimodal distribution and unidentified

water, these results reveal the existence of a positive charge distribution to the DMEM stock that can reduce the negative charges from FBS in the DMEM + 10% FBS samples as shown in the table of Fig. 1e. UV–vis spectroscopy (Fig. 1d) showed absorbance superposition from the biomolecules of DMEM and FBS, indicating stable agglomerates without aggregation in the supplemented DMEM sample.

Corona Formation Study

It is known that when AgNPs are in contact with biological fluids, its surface is quickly covered by the components of the fluid [9], forming a biomolecular corona [11, 39]. The behavior of biological molecules at the material interface is largely driven by the physico-chemical properties of the surface which is different not only among different nanomaterials but also within a set of the same materials variously prepared or modified [12]. In this study, the AgNP-biomolecule complexes formed in DMEM, FBS, and DMEM + 10% FBS, three of the most used nutritional solutions to maintain cell basal metabolism, were investigated at 37 °C.

As shown in Fig. 1b, the nutritional environment introduced a large variety of proteins and bioprotein aggregates of different sizes. Because of interference from culture media scattering, using DLS in situations with high molecule concentrations and low AgNP concentrations is difficult, and the results should be carefully reviewed before drawing conclusions. It should also be pointed out that the fluorescence of components of the culture medium, such as phenol red ($\lambda_{ex} = 440$ nm) or amino acids ($\lambda_{ex} = 280$ nm) in the samples, are factors that can contribute to lowering the intensities of scattered light in DLS, reducing the S/N ratio and thus presenting the potential to produce artificially smaller sizes [40]. To support our findings, some experimental actions were performed to prevent misinterpretation of the DLS data [40] for instance, centrifugation at 14,500 rpm for 15 min to remove the unbound molecules. For DLS measurements, 20 runs per triplicate sample were used, with a laser of 532 nm and a fixed angle of 90° for all obtained curves [41]. All measurements presented in this work underwent a review of the device itself and were considered of "good quality" [40], showing peaks distinguishable from the background signal.

On the other hand, because of the sample strategy employed in this study, it was necessary to assume some degree of uncertainty in these experiments, but this did not compromise the integrity of our hypothesis once the proposed model was built from experiments such as SAXS, UV–vis, SSF, and TRF. For instance, the main solvents used to prepare the samples in this study contained ultrapure water, sodium bicarbonate, and citric acid, which did not interfere with the viscosity of the samples, contributing to the prevention of significant pH fluctuations due to the buffers' effect (maximum calculated SD of 0.4).

AgNPs-FBS Interactions

The protein corona formation was monitored when the AgNPs stock solution was diluted in FBS to obtain 25 µM Ag in 70.6 µM protein, 50 µM Ag in 62.8 µM protein, 75 µM Ag in 54.9 µM protein, and 100 µM Ag in 47.1 µM protein, and incubated for 24 and 48 h. Figure 2 summarizes the main results obtained from the DLS (Fig. 2a-b), ZP (Fig. 2c), and UV–vis experiments (Fig. 2d).

The particle size distribution results for 25, 50, 75, and 100 µM silver incubated for 24 and 48 h, shown in Fig. 2a, exhibited high-intensity peaks that clearly masked the characteristic nanoparticle size distribution pattern. Compared to the AgNPs stock peak, we observed that these concentrations presented a slight shifting towards larger diameters, reaching a maximum values at 46.3 ± 0.4 nm for 24 h and 51.2 ± 1.1 nm for 48 h to 25 µM Ag in 70.6 µM protein as shown in the table of Fig. 2e. Similarly, the autocorrelation function shown in Fig. 2b, for all silver concentrations, decays slightly slower than AgNPs stock, indicating a shift to larger species. The ZP and UV–vis data in Fig. 2c-d suggests that the formation of large species observed by DLS was probably due to the adsorption of protein components of FBS onto the nanoparticles to form the protein corona. In relation to the AgNPs stock data, the zeta potential showed a reduction in its values from 13 to 15 mV during 24 and 48 h (table of Fig. 2e), and the UV–vis experiments showed a slight red shift of the silver LSPR band from 4 to 5 nm during 24 and 48 h (table of Fig. 2e).

UV–Vis absorption spectroscopy was used to probe the interactions between FBS proteins and AgNPs. The absorbance of 75 µM Ag was monitored at 418 nm (λ_{max} and exclusive LSPR absorption of AgNPs shown in Fig. 1d) in the absence and presence of FBS concentration previously used (47.1 – 70.6 µM proteins) after 24 and 48 h of incubation at 37 °C. To calculate the apparent association constant (K_{app}) using the Benesi-Hildebrand equation (Supplementary Information, section Benesi–Hildebrand equation), we only considered FBS proteins that were accessible for bonding. The suspensions were centrifuged at 14,500 rpm for 20 min, unbound proteins in the supernatant were pipetted out, and the pellet was resuspended in ultrapure water. The fluorescence emission method was used to estimate the FBS protein concentration accessible for bonding [42]. For this purpose, the area under each tryptophan fluorescence curve was integrated and it was estimated that approximately 10% of the FBS proteins were available for bonding compared to the original concentrations (47.1 – 70.6 µM proteins).

An increase in the absorbance of AgNPs (Supplementary Fig. 2a of Supplementary Information) along with a red shift (4 – 5 nm) for 24 and 48 h indicated complex formation between FBS proteins and AgNPs [43]. From the Benesi-Hildebrand plot (Supplementary Fig. 2b of Supplementary Information), the apparent association constant (K_{app}) was determined as 1.15×10^3 L mol^{-1} for 24 h and 1.32×10^3 L mol^{-1} for 48 h. Sharma et al. [43] reported K_{app} values for the γ-globulin/AgNPs system between $10^5 - 10^6$ L mol^{-1}, higher than the K_{app} values found for FBS protein/AgNPs system of this work. The reason for this difference could be the stabilizer that we used. Studies have reported

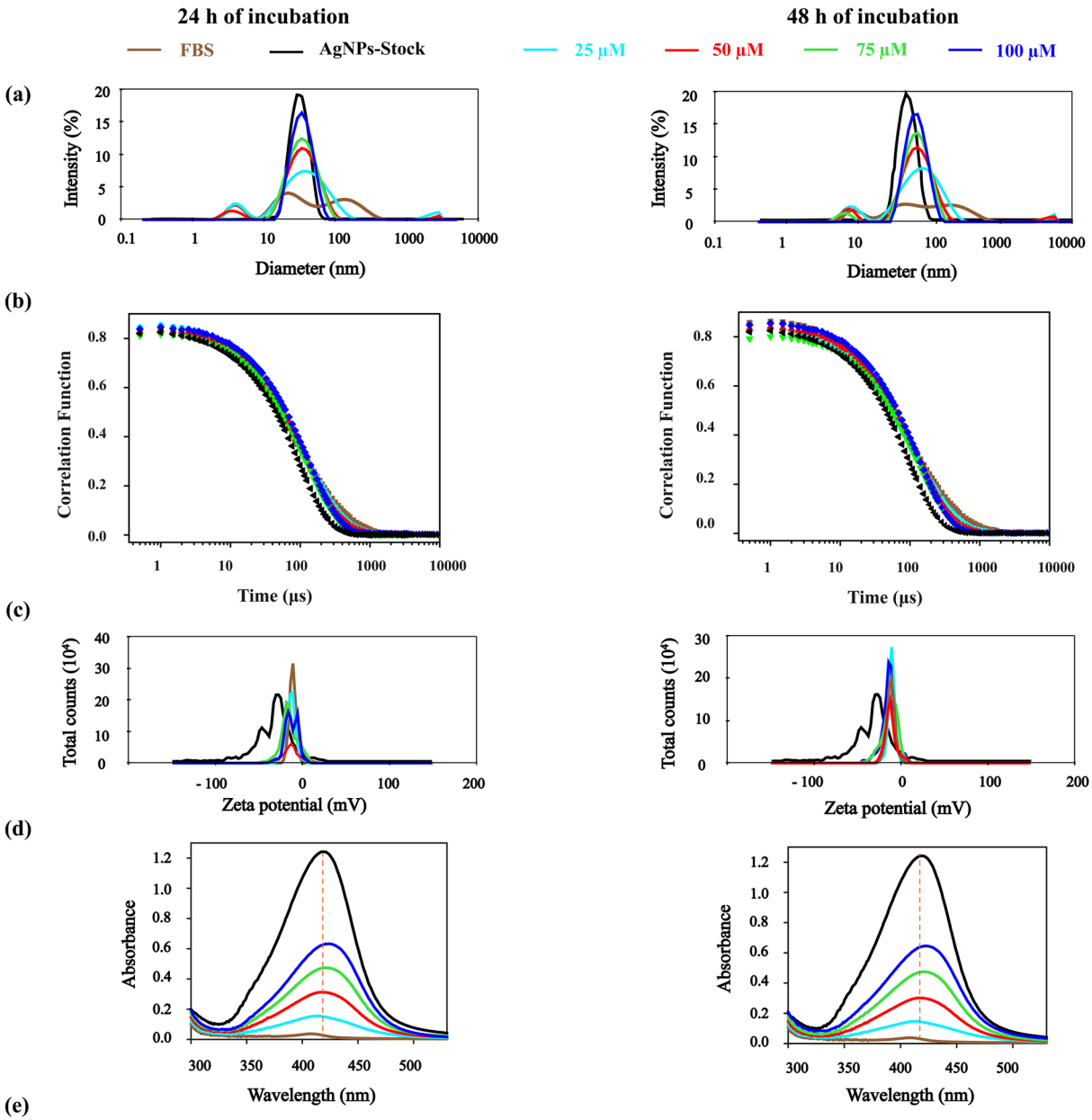

(e)

Sample (µM Ag)	DLS d (nm)	PDI	Zeta potential ζ (mV)	UV-vis λ max (nm)
AgNPs stock	41.7 ± 0.8	0.14 ± 0.01	- 33.6 ± 0.7	418 ± 2
25	46.3 ± 0.4	0.53 ± 0.02	- 13.6 ± 0.1	414 ± 3
50	44.9 ± 0.7	0.37 ± 0.04	- 15.5 ± 1.3	416 ± 2
75	44.8 ± 0.8	0.27 ± 0.01	- 15.7 ± 0.5	420 ± 1
100	43.5 ± 0.8	0.23 ± 0.03	- 14.2 ± 1.3	423 ± 1

Sample (µM Ag)	DLS d (nm)	PDI	Zeta potential ζ (mV)	UV-vis λ max (nm)
AgNPs stock	41.0 ± 0.5	0.10 ± 0.02	- 33.3 ± 0.3	420 ± 2
25	51.2 ± 1.1	0.52 ± 0.01	- 12.8 ± 1.3	414 ± 2
50	49.2 ± 1.0	0.38 ± 0.04	- 12.7 ± 0.2	416 ± 2
75	47.5 ± 0.5	0.27 ± 0.03	- 13.5 ± 0.5	421 ± 2
100	46.6 ± 1.4	0.22 ± 0.02	- 14.6 ± 0.2	424 ± 1

Fig. 2 Representative plots: **a** diameter distribution and **b** raw correlation function results obtained by DLS; **c** zeta surface potential results obtained from ZP measurements; and **d** optical absorption spectra acquired from UV–vis experiments. **e** Summary of the main results obtained from the characterization of the samples. Key: Plots at left for samples incubated for 24 h and at right for samples incubated for 48 h; black lines for AgNPs diluted in sodium citrate (stock); brown for FBS; and cyan, red, green, and blue for AgNPs diluted in FBS at 25, 50, 75, and 100 µM, respectively. Abbreviations: PDI, polydispersity index

that the hydrophilic surface of ligands can lead to the formation of water shells around nanoparticles, making protein adsorption poorly accessible [44]. In this scenario, it is very likely that the low K_{app} values and low thickness of the protein corona shown by DLS measurements could be due to the hydrophilic properties of the citrate ligand, inducing such water shells. In addition, the negatively charged surface of the AgNPs [45, 46] obtained in the ZP measurements, as shown in the table of Fig. 2e, corroborate these findings.

AgNPs-DMEM Interactions

The results obtained through DLS, ZP, and UV–vis experiments for the AgNPs stock diluted in DMEM to obtain solutions of 25 μM Ag in 160 mM biomolecules, 50 μM Ag in 140 mM biomolecules, 75 μM Ag in 120 mM biomolecules, and 100 μM Ag in 100 mM biomolecules, incubated for 24 and 48 h, clearly showed changes in the morpho-electrical characteristics of the nanoparticles as shown in Fig. 3. Surprisingly, the particle size distribution and raw autocorrelation results (Fig. 3a-b) show that, independent of the difference in molar concentration or incubation time, biomolecules from DMEM induced the formation of large species for 25, 50, 75, and 100 μM silver with average diameters of approximately 1598 ± 213 nm for 24 h and 1444 ± 452 nm for 48 h. From the UV–vis spectra and turbidity images (Fig. 3c-d), we observed that the characteristic LSPR peak of AgNPs (418 nm) disappeared, the color of the nanoparticle solution changed from yellow to black immediately after mixing with DMEM, and the precipitates appeared almost immediately. The DLS diameters and background in the absorbance signals increased with increasing AgNPs concentration for 24 and 48 h as shown in Fig. 3a-c, indicate scattering light from large agglomerates formed between the silver nanoparticles and biomolecules from DMEM [47, 48]. Similar observations have been reported for the RPMI medium inducing large agglomerates formation [49]. Regarding the zeta potential, the measurement apparatus was not able to detect any effective surface potential charges for this type of sample because of the darkness of the obtained solutions, which blocked the incident light and thus did not reach the detector.

Previous studies have demonstrated that the formation of the bio-corona depends on the protein concentration, association and dissociation rates, and surface charges [36, 50]. Interestingly, our results do not show corona formation; however, at low concentrations of DMEM (100 mM) or 100 μM silver ions, agglomeration was triggered to form large AgNP/biomolecule aggregates [51]. Similar observations have been reported for the fibrinogen protein inducing large agglomerates formation of silver and gold nanoparticles and in carbon nanotubes, indicating that this could be due to the unique molecular dimensions of fibrinogen [15]. In this sense, it can be argued that the large agglomerates and precipitation observed for AgNPs stock diluted in DMEM could be due to the positive charges of the individual biomolecules that compose DMEM, which could be rapidly attracted to the negative surface of AgNPs.

AgNPs–DMEM + 10% FBS Interaction

The SAXS, UV–vis, DLS, and ZP results about the interactions between AgNPs and bioproteins agglomerates had been reported earlier (Supplementary Figs. 1 and 2 in references [5, 6], respectively, 25 μM Ag in 160.1 mM bioprotein, 50 μM Ag in 140.1 mM bioprotein, 75 μM Ag in 120.0 mM bioprotein, and 100 μM Ag in 100.0 mM bioprotein, after 24 and 48 h of incubation). However, because it has not been thoroughly explored previously, the analysis of these data is offered here in greater depth, as shown in Table 2.

SAXS analyses for 25, 50, 75, and 100 μM after 24 and 48 h of incubation indicated that AgNPs presented similar values to the AgNPs stock with radius around 14.0 ± 5.0 nm (Table 2). In contrast, the analysis of the particle size distribution (Table 2) and raw correlation functions (Supplementary Fig. 3 of Supplementary Materials) obtained in DLS measurements reveals a tendency to increase AgNPs sizes compared to the stock ones. As can be seen in this Table 2, after 24 h of incubation, the average diameter of nanoparticles tends to increase in comparison to stock nanoparticles reaching a maximum diameter at 90.8 ± 11.0 nm to 25 μM Ag in 160.1 mM bioprotein. The morphological behavior after 48 h reproduces the general tendency found for 24 h of incubation being the average diameters of all mixtures larger than of stock nanoparticles, starting with, 190.6 ± 5.9 nm for 25 μM Ag in 160.1 mM bioprotein, until, 78.0 ± 1.7 nm for 100 μM Ag in 100.0 mM bioprotein as shown in the Table 2. The size differences observed between the DLS results with respect to SAXS results are not in disagreement but instead reveal the presence of an interesting mechanism of new "nanoparticle" growth. SAXS is related to the electron density between AgNPs and the culture medium [32, 52]. Therefore, since the contrast is much higher for silver than for the proteins in the culture medium, SAXS mainly detects AgNPs nuclei. On the other hand, DLS quantifies the average diffusion coefficient of the particles and, the larger the particle, the slower the diffusion [53]. In this sense, SAXS revealed that the core of AgNPs remained monodisperse in supplemented DMEM and DLS indicated the accumulation of bioprotein agglomerates from the culture medium around the nanoparticles, forming a "biomolecular corona," which grows in size as a function of molar concentration and time, as shown in Table 2 for the ΔR values. The reduction in zeta potential values from 27 to 30 mV and the slight red shift of the silver LSPR band from 3 to 4 nm with respect to the stock nanoparticle for both times (Table 2) again indicate the

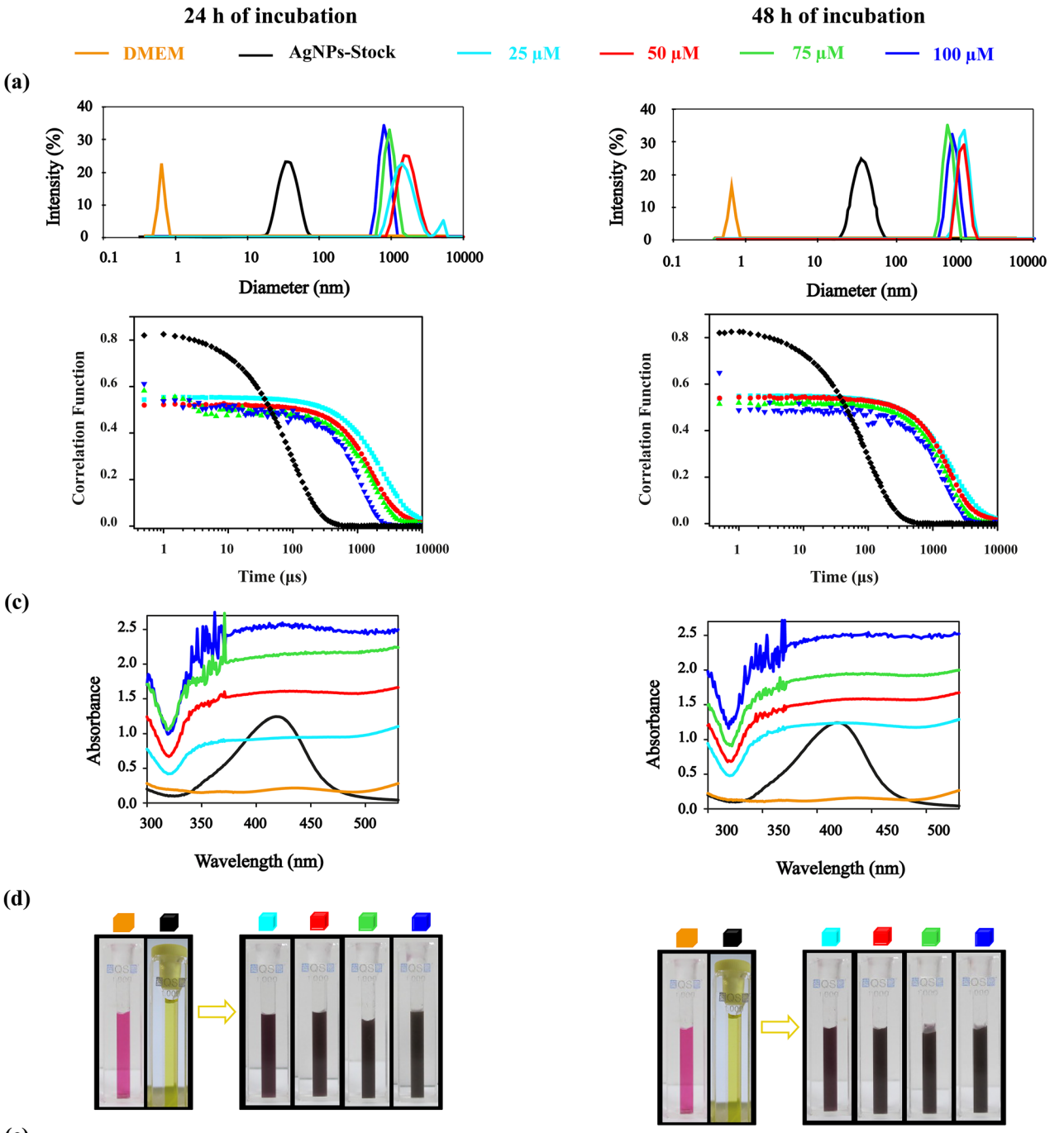

(e)

Sample (µM Ag)	DLS d (nm)	PDI	UV-vis λ max (nm)
AgNPs stock	41.7 ± 0.8	0.14 ± 0.01	418 ± 1
25	1598 ± 213	0.27 ± 0.01	n.i.
50	1351± 312	0.29 ± 0.02	n.i.
75	894 ± 116	1.00 ± 0.00	n.i.
100	1034 ± 168	1.00 ± 0.00	n.i.

Sample (µM Ag)	DLS d (nm)	PDI	UV-vis λ max (nm)
AgNPs stock	41.0 ± 0.5	0.10 ± 0.02	420 ± 1
25	1133 ± 109	0.14 ± 0.01	n.i.
50	1213 ± 284	0.15 ± 0.01	n.i.
75	1109 ± 161	1.00 ± 0.00	n.i.
100	1444 ± 452	1.00 ± 0.00	n.i.

◂**Fig. 3** Representative plots: **a** diameter distribution and **b** raw correlation function results obtained by DLS; **c** optical absorption spectra acquired from UV–vis experiments; and **d** turbidity images. **e** Summary of the main results obtained from the characterization of the samples. Key: Plots at left for samples incubated for 24 h and at right for samples incubated for 48 h; black lines for AgNPs diluted in sodium citrate (stock); dark yellow for DMEM; and cyan, red, green, and blue for AgNPs diluted in DMEM at 25, 50, 75, and 100 μM, respectively. Abbreviations: PDI, polydispersity index and n. i. indicate unidentified

adsorption of bioprotein components of culture medium onto the nanoparticles to form the protein corona.

To probe the interactions between bioprotein aggregates and AgNPs, we performed UV–vis absorption experiments, where the absorbance of 75 μM Ag was monitored at 418 nm (λ_{max} and exclusive LSPR absorption of AgNPs, as shown in Fig. 1d) in the absence and presence of DMEM + 10% FBS concentration previously used (100.0 – 160.07 mM bioproteins) after 24 and 48 h of incubation at 37 °C. The absorption spectra of AgNPs in the absence and presence of bioproteins are shown in Fig. 4a. The maximum absorption wavelength of AgNPs was approximately 422 – 424 nm for 24 and 48 h, and its intensity clearly increased as the concentration of bioproteins also increased. This is because of the complex formation between AgNPs and bioproteins [43].

To evaluate the binding between AgNPs and bioproteins, the apparent association constant (K_{app}) was calculated using a Benesi-Hilderband plot (Supplementary Information, section Benesi-Hilderband equation). For this purpose, the concentration of bioproteins available for bonding was estimated to be approximately 0.1% of the original concentrations (100.0 – 160.1 mM bioproteins), as described in Section "AgNPs-FBS Interactions". According to the Benesi-Hildebrand plot (inserts of Fig. 4a), the K_{app} values obtained after 24 and 48 h were $5.89 \times 10^5\,\mathrm{L\,mol^{-1}}$ and $3.95 \times 10^5\,\mathrm{L\,mol^{-1}}$, respectively.

From the K_{app} and ΔR values reported for DMEM + 10% FBS/AgNPs, we can observe that this system presents a better arrangement to adhere molecules around nanoparticles in relation to FBS/AgNPs, showing a larger corona radius (Table 2) and greater binding (Fig. 4b). This may be because the citrate stabilizer loses its hydrophilic property [44]. Studies have reported that hydrophilic ligands lose their adsorbed water around the nanoparticles under highly saline conditions [54], which occurs with DMEM + 10% FBS that presents a higher concentration of salt molecules (163 mM) than other biomolecules in solution. In this sense, it is possible to suggest that when nanoparticles were incubated in supplemented culture media, the first molecules to adhere to the surfaces of AgNPs, changing the negative surface to a positively charged salty surface, were possibly the different inorganic salts present in DMEM. These new salt shells could stimulate the increased adsorption of bioprotein agglomerates on their surfaces, producing a larger ΔR corona radius, as shown in Table 2. In fact, studies have reported that nanoparticles with positive surface charge attract more proteins when compared to negatively charged nanoparticles [45, 46]. The Fig. 4c illustrates the pictorial 3D-model that was proposed to illustrate the formation of biocoronas structures.

Fluorescence Study of Bioprotein-AgNPs Corona

Because DMEM/AgNPs presented an aggregation system and the FBS/AgNPs complex, compared to DMEM + 10% FBS/AgNP, presented low adsorption of molecules around the NPs, fluorescence measurements were only used to investigate the adsorption process of bioproteins from supplemented DMEM with AgNPs [9]. Among aromatic acids, tryptophan is the dominant intrinsic fluorophore [55]. This intrinsic fluorescence feature of DMEM + 10% FBS demonstrates the high sensitivity of tryptophan to its local microenvironment. Therefore, upon excitation at a specific wavelength, changes in the fluorescence emission spectra of tryptophan frequently occur due to conformational changes, ligand binding, or any externally added quenchers, such as nanoparticles [56].

The fluorescence data acquired at 37 °C and 280 nm of excitation wavelength, summarized in the Supplementary Fig. 4b of Supplementary Information, revealed that the sample 10% FBS showed an emission band in the interval between 300 – 550 nm with strong intensity at 344 nm due to its tryptophan residues [36], whereas the DMEM presented a much lower fluorescence intensity around 334 and 344 nm due to its tryptophan residues [55]. When excited under the same conditions, DMEM + 10% FBS showed a fluorescence emission intensity comparable to that of FBS, peaking at 344 nm (Supplementary Fig. 4b of Supplementary Information), however AgNPs stock did not exhibit any fluorescence emission in the experimental wavelength range. Based on these results, we can demonstrate that the fluorescence data presented in Fig. 5a for 25, 50, 75, and 100 μM of silver after 24 and 48 h of incubation and at 37 °C (310 K) mainly reflected the information of tryptophan from FBS (bio-FBS tryptophan), and that the interference from silver and tryptophans from DMEM could be neglected. A constant amount of DMEM + 10% FBS (100.0 mM bioprotein) was used in the preparation of these samples, but increasing concentration of AgNPs (25 – 100 μM) as informed before.

Analyzing Fig. 5a, after 24 and 48 h of incubation, as the molar concentration of silver increased in the supplemented DMEM solutions, the inner filter correction fluorescence intensity of bio-FBS tryptophans decreased in a concentration-dependent manner. These results suggest that the surface AgNPs available for bonding may interact with

Table 2 Summary of the main results obtained from the characterization of the samples of 25 μM Ag in 160.07 mM bioprotein, 50 μM Ag in 140.1 mM bioprotein, 75 μM Ag in 120.0 mM bioprotein, and 100 μM Ag in 100.0 mM bioprotein, after 24 and 48 h of incubation. Comparing the DLS and SAXS results, we estimated the thickness of the rich corona in biological molecules around the AgNPs since the radius of the nanoparticle core, 17.0 ± 2.0 nm, and citrate, 4.0 ± 1.0 nm, has the same average size, $R_{AgNPs\text{-}stock} = 21.0 \pm 0.4$ nm, during all the processes. Thus, we can estimate the thickness from the differences in the hydrodynamic values of the radius, that is, $\Delta R = R_{bio\text{-}AgNPs} — R_{AgNPs\text{-}stock}$., after 24 and 48 h of incubation

Sample (*μM* Ag)	**Incubation time**					
	24 h					
	SAXS *r (nm)*	***DLS*** *d (nm)*	***PDI***	***ZP*** *(mV)*	***UV–vis*** λ_{max}*(nm)*	***ΔR*** *(nm)*
AgNPs stock	17.0 ± 2.0	41.7 ± 0.8	0.14 ± 0.01	-33.6 ± 0.7	418 ± 1	0
25	14.1 ± 4.0	90.8 ± 11.0	0.34 ± 0.08	-6.7 ± 1.3	420 ± 2	24.5 ± 3.1
50	14.4 ± 5.0	88.5 ± 19.9	0.26 ± 0.02	-7.3 ± 1.5	421 ± 3	23.4 ± 1.1
75	14.8 ± 3.0	57.2 ± 1.6	0.28 ± 0.01	-5.9 ± 1.3	420 ± 4	17.8 ± 2.3
100	14.0 ± 4.0	61.4 ± 1.2	0.24 ± 0.01	-6.3 ± 1.2	420 ± 2	10.6 ± 2.0
	48 h					
AgNPs stock	18.0 ± 1.0	41.0 ± 0.5	0.10 ± 0.02	-33.3 ± 0.3	420 ± 1	0
25	13.4 ± 4.0	170.6 ± 5.8	0.48 ± 0.02	-1.8 ± 0.3	420 ± 4	54.4 ± 3.0
50	14.6 ± 3.0	141.4 ± 2.0	0.25 ± 0.01	-3.4 ± 0.3	421 ± 3	49.9 ± 2.1
75	14.7 ± 4.0	97.5 ± 1.6	0.16 ± 0.01	-4.7 ± 1.4	424 ± 2	28.0 ± 1.8
100	14.0 ± 3.0	78.0 ± 1.7	0.12 ± 0.02	-3.4 ± 0.3	421 ± 3	18.2 ± 1.1

bioprotein aggregates and act as quenchers to decrease the fluorescence intensity of tryptophan.

A decrease in the fluorescence intensity is called quenching, which may be attributed to a dynamic or static interaction between the fluorophore and the quencher [56]. Dynamic quenching stems from collisions between the quencher and the fluorophore during the lifetime of the excited state. Upon contact, the fluorophore in its excited state loses its excited energy and returns to the ground state, resulting in fluorescence quenching [36]. Static quenching results from the formation of a new non-fluorescent complex between the fluorophore and quencher [18]. Because the intrinsic fluorescence of bio-FBS tryptophans may be quenched by surface silver nanoparticles and to further elucidate the quenching mechanism, the fluorescence quenching data were analyzed using the Stern–Volmer equation [19] as follows.

$$F_0/F = 1 + K_{SV}[Q] = 1 + k_q\tau_0[Q]$$

where F_0 and F are the steady-state fluorescence intensities in the absence and presence of the quencher, respectively; K_{SV} is the Stern–Volmer constant; and $[Q]$ is the quencher concentration (surface AgNPs). The surface AgNP concentrations were obtained considering that only 4% of the surface atoms were accessible for bonding from a stock concentration of 250.3 μM silver in the solution (Supplementary Materials, section "Calculation of 4% of surface atoms accessible for binding"). In this sense, 4 μM (rather than 100 μM), 3 μM (rather than 75 μM), 2 μM (rather than 50 μM), and 1 μM (rather than 25 μM) were utilized in the equation [57–59]. Parameters k_q and τ_0 are the bimolecular quenching rate constant and fluorophore lifetime in the absence of a quencher, respectively. The τ_0 bio-FBS tryptophans were obtained from the time-resolved fluorescence experiment as 1.82 ± 0.26 ns for 24 h and 1.79 ± 0.19 ns for 48 h.

The corrected Stern–Volmer plots of the fluorescence quenching of bio-FBS tryptophans induced by surface AgNPs at three different temperatures (300, 305, 310, and 315 K), after 24 and 48 h of incubation, are shown in Fig. 5b. A good linear relationship between the plots for 24 and 48 h is presented after using the Stern–Volmer equation to perform the correction. The Stern–Volmer plots revealed a linear relationship, indicating that only one type of quenching mechanism could exist, dynamic or static. One method to distinguish between dynamic and static quenching is to investigate the effects of temperature on the interactions of AgNPs with bioprotein aggregates. In dynamic quenching, a higher temperature results in a faster diffusion rate and higher quenching constant (K_{SV}) [43]. In static quenching, higher temperatures result in dissociation of the bound complex, thus reducing the quenching constant [43]. Another distinction between dynamic and static quenching is the k_q value. Because dynamic quenching mainly depends on collision, its k_q value is normally limited to the maximum bimolecular quenching constant of 2×10^{10} mol^{-1} s^{-1} [18]. If the value of k_q is greater than 2×10^{10} mol^{-1} s^{-1}, it indicates that the quenching mechanism is mainly static quenching [19]. The K_{SV} values obtained from the slopes of these plots for 24

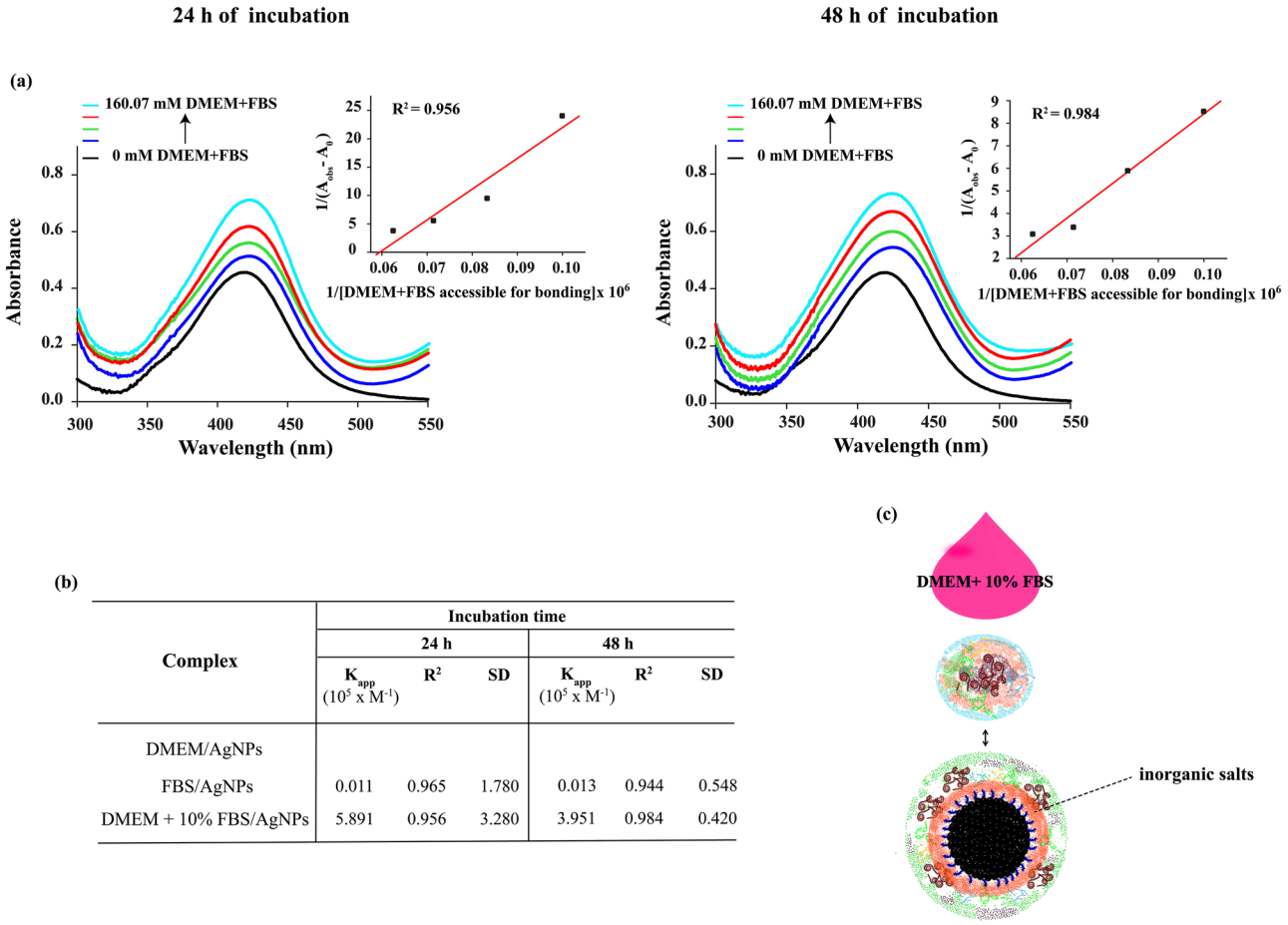

Complex	Incubation time					
	24 h			48 h		
	K_{app} (10^5 x M^{-1})	R^2	SD	K_{app} (10^5 x M^{-1})	R^2	SD
DMEM/AgNPs						
FBS/AgNPs	0.011	0.965	1.780	0.013	0.944	0.548
DMEM + 10% FBS/AgNPs	5.891	0.956	3.280	3.951	0.984	0.420

Fig. 4 **a** Absorbance spectra of AgNPs (75 μM) with bioprotein (100.0 – 160.1 mM). Inserts: Benesi-Hildebrand plot for complexation between bioproteins and AgNPs, considering that approximately 0.1% of the bioproteins were available for bonding compared to the original concentrations. **b** Apparent association constants K_{app} for the interactions of the AgNPs with molecules from DMEM, FBS and DMEM + 10% FBS. **c** Schematic illustration of the bioprotein/AgNP interactions and protein corona formation phenomena

and 48 h of incubation are listed in Table 3. As can be seen, the K_{SV} values decreased with increasing temperature and the values of k_q were greater than the limiting diffusion rate constant of the biomolecules (2×10^{10} mol^{-1} s^{-1}), indicating that the quenching mechanism of bio-FBS tryptophans by surface AgNPs is mainly static quenching.

The ultimate method for distinguishing between static and dynamic quenching is the measurement of fluorescence lifetimes [36]. Therefore, the quenching mechanisms for the interaction of AgNPs surface with bioproteins aggregates were further confirmed by lifetime measurements in this work. The time-resolved fluorescence curves for 25, 50, 75, and 100 μM silver and supplemented DMEM after 24 and 48 h of incubation at 37 °C are presented in Fig. 5c. As shown in the figure, there was no discernible difference in the decay curves of bio-FBS tryptophan with increasing molar concentration of AgNPs. Surface AgNPs had little effect on the fluorescence lifetime of bio-FBS tryptophan, which was the sum of the exponential decay, χ^2, close to 1.00, for all silver concentrations (Table 4). For static quenching, the fluorescence lifetime of the fluorophore is not affected during complex formation [36]. Consequently, it can be concluded that the quenching mechanism of bio-FBS tryptophan by the silver nanoparticles is static quenching, which is due to the adsorption of bioproteins on the surface of AgNPs and the formation of the corona as shown in Fig. 4d.

For the static quenching process, under the assumption that bioprotein agglomerates and AgNPs from the surface form a stable complex, the binding parameters, K_b and n, may be calculated using a double logarithmic plot through the following equation [19]

$$\log((F_0 - F)/F) = \log(K_b) + n.\log([Q])$$

where the binding constant K_b predicts the stability of the complex and the binding number n the degree of

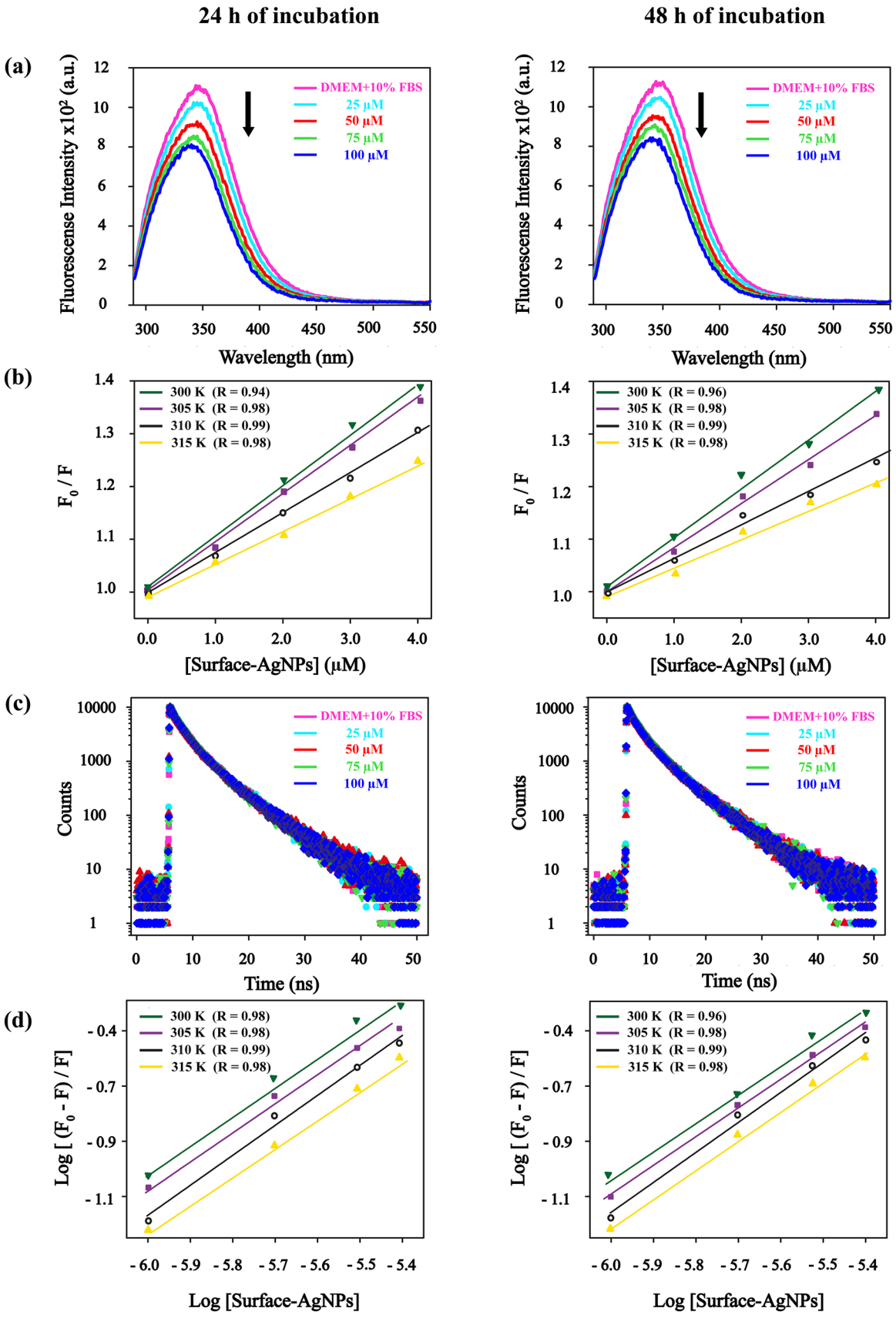
24 h of incubation
48 h of incubation
(a)
Fluorescense Intensity x10² (a.u.)
Wavelength (nm)
DMEM+10% FBS
25 µM
50 µM
75 µM
100 µM
(b)
F₀ / F
[Surface-AgNPs] (µM)
300 K (R = 0.94)
305 K (R = 0.98)
310 K (R = 0.99)
315 K (R = 0.98)
300 K (R = 0.96)
305 K (R = 0.98)
310 K (R = 0.99)
315 K (R = 0.98)
(c)
Counts
Time (ns)
(d)
Log [(F₀ - F) / F]
Log [Surface-AgNPs]

◂**Fig. 5** Representative plots **a** Steady-state fluorescence emission spectra; **b** Stern–Volmer plot; **c** time-resolved fluorescence decay profile; and **d** double logarithmic plots for the bio-FBS tryptophan of DMEM + 10% FBS in the absence and presence of AgNPs after 24 and 48 h of incubation. Key: Pink lines for DMEM + 10% FBS (constant amount of 100 µM bioprotein); cyan, red, green, and blue for AgNPs diluted in supplemented DMEM at 25, 50, 75, and 100 µM, respectively. For Steady state and time-resolved fluorescence the results are presented at 37 °C (310 K), whereas for Stern–Volmer and double logarithmic plots the quenching fluorescence at 300, 305, 310 and 315 K with the molar concentration of silver atoms in surface available for bonding, 4 µM, 3 µM, 2 µM and 1 µM. Excitation at λ_{ex} = 280 nm for Steady-state Fluorescence. Excitation at λ_{ex} = 280 nm and emission at λ_{em} = 350 nm for time-resolved fluorescence

cooperativity with which the protein binds to the surface of AgNPs [19].

The results of binding parameters for 24 and 48 h, summarized in Fig. 6d and Table 3, indicated that the bioprotein/AgNP system presented binding affinities of K_b order of magnitude 10^5 M^{-1}. At 37 °C, we can observe that K_b matches the results of the UV–visible spectra study at 5.89×10^5 M^{-1} and 3.28 10^5 M^{-1} for 24 and 48 h respectively. The *n*-values were obtained approximately equal to 1, indicating a positive cooperative interaction and bioprotein aggregates presenting only a single binding site for AgNPs [36]. Sharma et al. [43] and Waghmare et al. [19], reported K_b values for the γ-globulin/AgNPs and albumin/AgNPs systems in the magnitude order of 10^5 – 10^{12} M^{-1}, which was higher than the bioprotein/AgNPs system obtained in this work. The reason could be the borohydride stabilizer and the 50 nm nanoparticles that they used [19, 43]. In fact, Wang et al. [60] showed that different stabilizers (citrate, cysteine, PEG, and CTAB) and NPs sizes in the Albumin/AuNP system presented K_b values in the magnitude order of 10^8 – 10^{10} M^{-1}. In conclusion, we believe that K_b is related to the particle size of AgNPs, synthesis methods, and quencher-protein systems.

The increase of K_b values with the increase of temperatures indicates that the interaction between the bioprotein aggregates and AgNPs surface is endothermic. The results were validated by enthalpy change as shown in the Supplementary Fig. 5 and Supplementary Table 2 of Supplementary Information. The incubation of the bioprotein/AgNP system at 37 °C (310 K) to simulate the cellular environment resulted in a slight decrease in the binding constant K_b for 48 h when compared with 24 h. It is known that proteins with higher binding affinities form the ‘‘hard” corona that is more tightly bound to the surface as compared to the lower binding affinities ‘‘soft” corona forming proteins [61]. In this sense, the K_b values at 48 h could corroborate our assumption that the increase in bioproteins aggregates on the surface of the nanoparticles after 48 h of incubation is characterized by soft coronas.

The thermodynamic parameters used to study the interaction forces involved at the interface of the biocorona, as well as the mode of interaction between bioprotein aggregates and AgNPs, can be $\Delta H > 0$ and $\Delta S > 0$, through hydrophobic forces; $\Delta H < 0$ and $\Delta S < 0$, van der Waals interactions and hydrogen bonds; $\Delta H > 0$ and $\Delta S < 0$, electrostatic interaction [62]. If the thermodynamic parameters ΔH (enthalpy change) and ΔS (entropy change) undergo slight changes over the investigated temperature range, ΔH and ΔS can be determined using the van't Hoff equation.

$$\log(K_b) = - \triangle H/RT + \triangle S/R$$

where K_b is the binding constant at the corresponding temperature, T is the temperature in Kelvin, and R is the gas constant (8.3144621 J/molK). The thermodynamic parameters are derived from the slope and intercept of the linear van't Hoff plots. The Gibbs free energy ΔG can be calculated as

$$\triangle G = \triangle H - T. \triangle S$$

The van't Hoff plot was used for the interaction of bioprotein aggregates and AgNPs surface at the corresponding temperatures (Supplementary Fig. 5), and the thermodynamic parameters are presented in Supplementary Table 1 of Supplementary Materials. The negative Gibbs free energy (ΔG) changes at -34.1 kJ/mol for 24 h and at -32.8 kJ/mol for 48 h of incubation times, indicating the spontaneity of the binding of bioprotein aggregates to the AgNPs surface. The change in enthalpy of the corona at 26.7 kJ/mol for 24 h and at 38.0 kJ/mol for 48 h represents an increase in intermolecular bond energies during the binding process, whereas the change in entropy following corona formation at 196.1 J/mol.K for 24 h and 228.5 J/mol.K for 48 h results in a change in the system disorder. We observed that $\Delta H > 0$ and $\Delta S > 0$, suggesting that the binding process is entropy-driven and endothermic. Hence, endothermic and entropy-driven processes are associated with hydrophobic forces [62]. In addition, the positive values of ΔH and ΔS contributed to the negative values of ΔG. Therefore, we conclude that hydrophobic interactions are probably the main forces in the binding of bioprotein aggregates to AgNPs from the surface and the interaction is driven by enthalpy and entropy. Similar behaviors were observed for the association between albumin and silver nanoparticles, γ-globulin, and hemoglobin with gold nanoparticles [18, 19].

Cytotoxicity of the AgNPs/bioprotein Complex

Current research results indicate that the inherent cytotoxicity of AgNPs may be a useful tool to control biological cell activities through its impact on metabolic functions during the cutaneous healing process [5, 6]. The biological response

Table 3 Binding and quenching parameters for complexation between bioproteins and AgNPs from the surface after 24 and 48 h of incubation times. Key: The parameters were calculated using the concentration of atoms available for bonding would be: 4 μM (instead of 100 μM), 3 μM (instead of 75 μM), 2 μM (instead of 50 μM) and 1 μM (instead of 25 μM)

Temp. (K/°C)	*Quenching parameters*				*Binding parameters*			
	K_{SV} (10^5 M^{-1})		k_q (10^{14} s^{-1} M^{-1})		K_b (10^5 M^{-1})		n	
	24 h	48 h	24 h	48 h	24 h	48 h	24 h	48 h
300 / 27	2.35 ± 0.04	2.21 ± 0.02	1.29 ± 0.04	1.23 ± 0.03	4.03 ± 0.11	2.04 ± 0.15	1.00 ± 0.02	1.02 ± 0.01
305 / 32	2.12 ± 0.09	2.04 ± 0.01	1.16 ± 0.03	1.13 ± 0.01	5.49 ± 0.10	2.83 ± 0.11	1.04 ± 0.01	1.02 ± 0.01
310 / 37	1.90 ± 0.07	1.67 ± 0.03	1.04 ± 0.03	0.93 ± 0.05	6.09 ± 0.25	3.56 ± 0.23	1.08 ± 0.07	1.05 ± 0.07
315 / 42	1.51 ± 0.03	1.37 ± 0.05	0.82 ± 0.02	0.76 ± 0.02	6.85 ± 0.12	4.23 ± 0.15	1.10 ± 0.02	1.07 ± 0.01

to nanoparticle cytotoxicity can be either enhanced or diminished by the size of the corona as well as the concentration and incubation time [25]. To evaluate the cytotoxic effect of the bioprotein/AgNP complex on cellular growth, we compared the cytotoxic response of microvascular endothelial cells (HUV-EC-C), human fibroblast cells (FN1), and murine macrophages (RAW 264.7) after protein corona formation.

The cellular growth results are presented in Fig. 6a as dose–response curves dependent on the concentration and cell exposition time obtained from Neubauer chamber assays. As can be seen when we plotted the number of viable cells as a function of AgNPs concentration, "$N_{cells} \times$ [AgNPs]" for 24 and 48 h, the bioprotein/AgNP cell exposure are inducing a systematic decrease in the number of cells as the increase the AgNPs concentration, indicating dose-dependent inhibition of cell proliferation and cell death, and thus demonstrating the effective cytotoxicity of AgNPs. When we calculate the percentage reduction of viable cells for each silver molar concentration, the obtained results revealed that the cell lineages showed different cytotoxic responses to exposure to nanoparticles, depending on the concentration and time of incubation. For instance, the results in Fig. 6b, demonstrated that [AgNPs] = 75 μM for 24 h and [AgNPs] = 50 μM for 48 h resulting in an average decrease of cell populations, relative to the control, of 50% and 47% for FN1, 57% and 54% for HUV-EC-C, and 45% for RAW 264.7. As can be seen in these data, the FN1 and HUV-EC-C cell lineages exhibited different changes in cell populations compared to RAW 264.7. This behavior is expected because cells would resist the cytotoxic effects of AgNPs in different ways, depending on their genetic potential [5, 6].

Although we did not conduct specific experiments to determine the exact mechanism of AgNPs toxicity, studies have indicated that it is produced by the process of AgNPs absorption by cells [63], which enables us to propose the following explanation. Because the bioprotein/AgNP complex is always the same in all cell lines, that is, they contain the same amount of AgNPs and have the same thickness as the bioprotein corona for each molar concentration in supplemented DMEM, we can expect these bioprotein agglomerates to have an affinity for the receptor proteins on the cell membrane [13, 64], as illustrated in Fig. 6c. Hence, the observed changes in cellular proliferation may be related to AgNPs cytotoxicity through the process of cell ingestion and subsequent release of silver ions into the cytosol, which would trigger the cytotoxic mechanism identified as dose- and time-dependent.

The morpho-electric characteristics and binding mechanism of the bioprotein/AgNP complex, related to their spherical size, positively charged salty surface [45, 46], endothermic and entropy processes in association with hydrophobic forces, seem to be important factors that define the degree of internalization of the bioprotein/AgNP complex inside of the cells, justifying themselves as key factors in cytotoxic studies [65]. The viability assays results revealed that concentrations in the range of 75 μM ≤ [AgNPs] ≤ 100 μM, where the bioproteins/AgNPs have smaller corona thicknesses (Table 2), tend to be more easily internalized by cells than larger thicknesses, triggering major changes in viable cells such as proliferation rates. Incubation time also contributes by affecting cells through cytotoxicity once the percentage

Table 4 Time-resolved parameters of the bio-FBS tryptophan of DMEM + 10% FBS in the absence and presence of AgNPs after 24 and 48 h of incubation at 37 °C. Key: 0 μM for DMEM + 10% FBS (constant amount of 100 mM bioprotein), and 25, 50, 75, and 100 μM for AgNPs diluted in DMEM + 10% FBS. τ is the fluorescence lifetime and the magnitude of χ^2 denotes the goodness of fit. Excitation at λ_{ex} = 280 nm and emission at λ_{em} = 350 nm

AgNPs *(μM)*	*Incubation time*			
	24 h		48 h	
	τ (*ns*)	χ^2	τ (*ns*)	χ^2
0	1.82 ± 0.26	1.32	1.79 ± 0.19	1.18
25	1.73 ± 0.19	1.31	1.70 ± 0.14	1.17
50	1.77 ± 0.24	1.29	1.71 ± 0.09	1.14
75	1.81 ± 0.19	1.25	1.75 ± 0.18	1.11
100	1.85 ± 0.14	1.16	1.64 ± 0.14	1.31

(a)

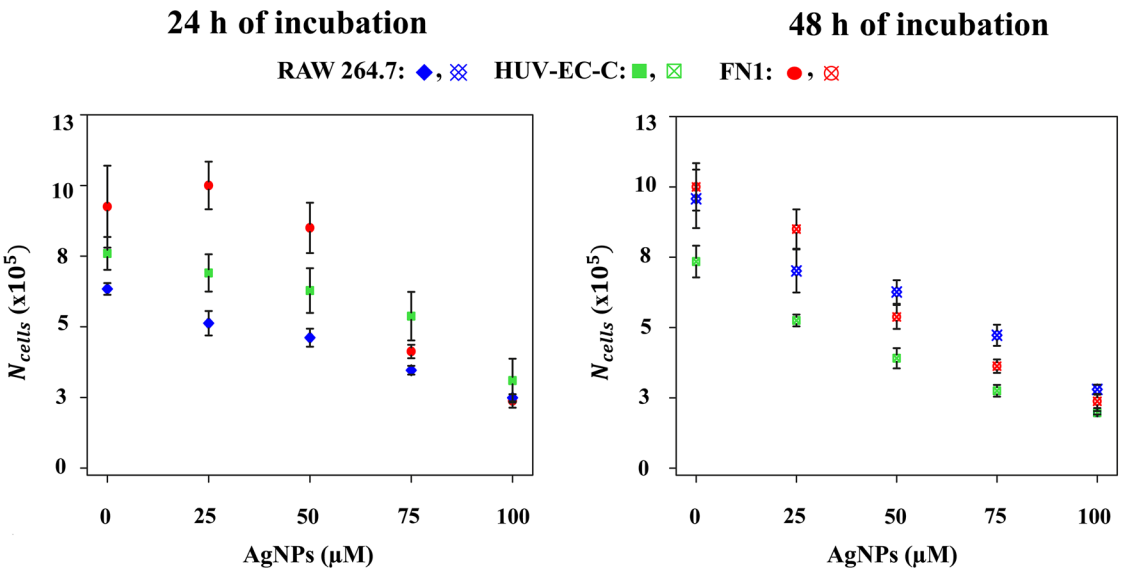

(b)

AgNPs (µM)	FN1 viable cells (%)	HUV-EC-C viable cells (%)	RAW 264.7 viable cells (%)
Incubation time: 24 h			
0	100 A	100 A	100 A
25	108 A +8%	86 B -14%	81 B -19%
50	91 B -10%	78 C -22%	73 C -27%
75	50 C -50%	43 D -57%	55 D -45%
100	26 D -75%	35 E -65%	40 E -60%
Incubation time: 48 h			
0	100 A	100 A	100 A
25	85 B -15%	71 B -29%	73 B -27%
50	53 C -47%	46 C -54%	55 C -45%
75	36 D -64%	36 D -64%	49 D -51%
100	23 D -77%	26 E -74%	29 E -71%

(c)

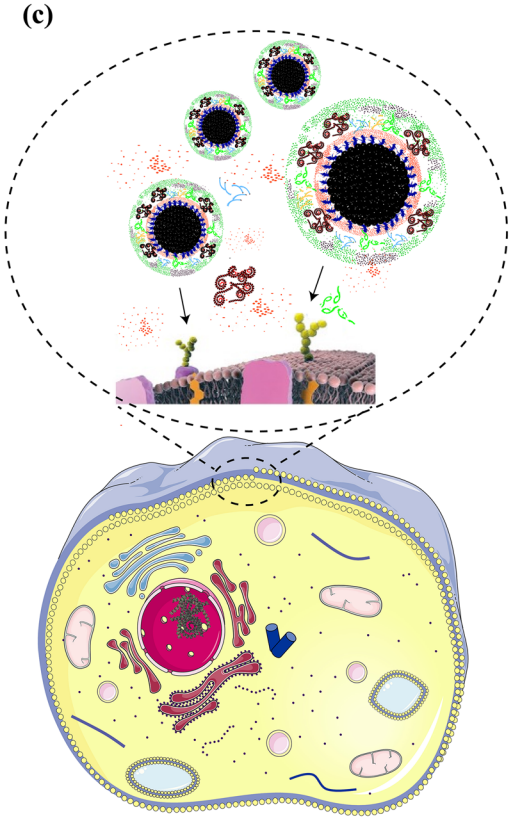

Fig. 6 **a** The number of viable cells counts in the Neubauer chamber and **b** general summary of statistical data analysis from univariate approaches, showing the percentage reduction of viable cells and lethality zone for FN1, HUV-EC-C and RAW 264.7 cells exposed to different silver molar concentrations and times of exposure. **c** Illustrative model of the process of internalization of the 3D bioprotein/AgNPs complex in cells through interaction with the cell membrane receptor proteins. Key: Viable cell levels were expressed as percentages and normalized considering the control sample (free nanoparticles) as 100% (values expressed in percentages). Arrows up and down show tendencies to increase or decrease levels, and the results are tabulated for different cell lineages. Different letters inserted below the percentage values indicate statistical differences by Fisher's pairing. The comparisons considered 95% as the confidence level parameter ($p < 0.05$)

of viable cells was significantly reduced at 48 h compared to 24 h. Although the bioproteins/AgNPs presented an increase in the corona thickness over the time (Table 2), the time-dependent cytotoxicity could be explained by the longer interaction time between the bioproteins and cell membrane receptor proteins, which also favors greater ingestion of the nanoparticles by cells. However, we have to be aware that longer incubation periods also imply depletion of cell culture medium components and thus contribute to cellular death.

To conclude, as concerning cytotoxicity, the cell lineages presented different dose intervals for distinct times, where they are losing half of their viable cell population. From this one point backward (to minor dosages), the possibility that these immortalized cell lineages can recover cell confluence remains latent once cell culture conditions free of nanoparticles are provided and regulated. Although this work does not provide assays that specifically address this question, the current argument remains plausible; therefore, we can use these intervals of cytotoxicity: [AgNPs] < 75 μM for 24 h and [AgNPs] < 50 μM for 48 h. These classifications, in principle, could help us control the cell population through the cytotoxic potential of bioprotein/AgNPs complex, which could be used to our advantage by promoting cell populations that will favor, for instance, in processes such as inflammation or remodeling during skin wound healing [5, 6].

Conclusions

In the present work, we investigated the morpho-electric characteristics of silver nanoparticles in DMEM, FBS and DMEM supplemented with 10% FBS at different molar concentrations and incubation times. We also investigated the binding mechanism of biomolecules and proteins adsorbed on AgNPs surfaces, as well as their cytotoxic effect in FN1, HUV-EC-C, and RAW 264.7 cell lineages. Our results suggest that the inorganic salts of DMEM help achieve a strong interaction between AgNPs and bioprotein aggregates of DMEM + 10% FBS, leading to the formation of biomolecular coronas around the nanoparticles, thus forming a new stable entity called bioproteins/AgNPs. This entity presents variations in corona size that depend on the concentration and incubation time, but not on the hard core of AgNPs. A pictorial 3D-model was proposed in order to illustrate the formation of biocoronas structures showing the different layers of molecules and silver nanoparticles as well as the order of the interactions among them, starting from proteins in the first shell, then the amino acids and organic salts that create a link between these proteins and the immutable hard core of the AgNPs. Additionally, binding constants of AgNPs from the surface with bioprotein aggregates were estimated in the range of 10^5 M^{-1} at 300, 305, 310, and 315 K. Besides, the thermodynamic analysis showed that hydrophobic interactions are the main interaction forces for the bioprotein/AgNP system and the interaction is driven by enthalpy and entropy. From a cytotoxicity point-of-view of biomolecular coronas, the studied cell lineages presented a systematic decrease in their population when the number of nanoparticles increases and the diameter of the corona decreases in the solutions of supplemented culture medium.

Supplementary Information The online version contains supplementary material available at https://doi.org/10.1007/s10895-023-03564-x.

Acknowledgments This work was supported by the Coordenação de Aperfeiçoamento de Pessoal de Nível Superior—Brasil (CAPES)—Finance Code 001. The authors would like to acknowledge the Butantan Institute for providing the human normal fibroblast cell lineage.

Author Contributions CVVP contributed to sample preparations, all assays, data processing, statistical analysis, data interpretations, and drafted the entire manuscript. ACB contributed to part of experiments, data interpretations, and general supervision of this work. ELD contributed to the Fluorescence, Absorbance, Zeta potential, and DLS experiments and data interpretations. YBB made suggestions and corrections to the manuscript. CLPO contributed to the small-angle X-ray scattering experiments and data analysis. SHT, JJS and KA provided the AgNP nanoparticles and contributed to the discussion of the results. All authors contributed to revising the manuscript and agreed to be fully accountable for ensuring the integrity and accuracy of the work and reading and approving the final manuscript.

Funding Coordenação de Aperfeiçoamento de Pessoal de Nível Superior,Finance Code 001

Availability of Data and Materials Not applicable.

Declarations

Ethical Approval Not applicable.

Competing Interests The authors have no relevant financial or non-financial interests to disclose.

References

1. Durán N, Durán M, de Jesus MB et al (2016) Silver nanoparticles: A new view on mechanistic aspects on antimicrobial activity. Nanomedicine 12:789–799. https://doi.org/10.1016/j.nano.2015.11.016
2. de Lima R, Seabra AB, Durán N (2012) Silver nanoparticles: a brief review of cytotoxicity and genotoxicity of chemically and biogenically synthesized nanoparticles. J Appl Toxicol 32:867–879. https://doi.org/10.1002/jat.2780
3. Hackenberg S, Scherzed A, Kessler M et al (2011) Silver nanoparticles: evaluation of DNA damage, toxicity and functional impairment in human mesenchymal stem cells. Toxicol Lett 201:27–33. https://doi.org/10.1016/j.toxlet.2010.12.001
4. Castiglioni S, Caspani C, Cazzaniga A, Maier JA (2014) Short- and long-term effects of silver nanoparticles on human microvascular endothelial cells. World J Biol Chem 5:457–464. https://doi.org/10.4331/wjbc.v5.i4.457
5. Palomares CVV, Barreto YB, Bexiga NM et al (2023) Metabolic profiling of murine macrophages exposed to silver nanoparticles

at dose and time dependencies. Part Part Syst Charact 2200191. https://doi.org/10.1002/ppsc.202200191
6. Vivas CV, dos Santos JA, Barreto YB et al (2023) Biochemical response of human endothelial and fibroblast cells to silver nanoparticles. Bionanoscience. https://doi.org/10.1007/s12668-023-01091-4
7. Lategan KL, Walters CR, Pool EJ (2019) The effects of silver nanoparticles on RAW 264.7. Macrophages and human whole blood cell cultures. Front Biosci (Landmark Ed) 24:347–365. https://doi.org/10.2741/4722
8. Tak YK, Pal S, Naoghare PK et al (2015) Shape-Dependent Skin Penetration of Silver Nanoparticles: Does It Really Matter? Sci Rep 5:16908. https://doi.org/10.1038/srep16908
9. Nel AE, Mädler L, Velegol D et al (2009) Understanding biophysicochemical interactions at the nano-bio interface. Nat Mater 8:543–557. https://doi.org/10.1038/nmat2442
10. García-Álvarez R, Hadjidemetriou M, Sánchez-Iglesias A et al (2018) In vivo formation of protein corona on gold nanoparticles. The effect of their size and shape. Nanoscale 10:1256–1264. https://doi.org/10.1039/c7nr08322j
11. Cedervall T, Lynch I, Lindman S et al (2007) Understanding the nanoparticle-protein corona using methods to quantify exchange rates and affinities of proteins for nanoparticles. Proc Natl Acad Sci USA 104:2050–2055. https://doi.org/10.1073/pnas.0608582104
12. Lundqvist M, Stigler J, Elia G et al (2008) Nanoparticle size and surface properties determine the protein corona with possible implications for biological impacts. Proc Natl Acad Sci USA 105:14265–14270. https://doi.org/10.1073/pnas.0805135105
13. Ma Y, Hong J, Ding Y (2020) Biological behavior regulation of gold nanoparticles via the protein corona. Adv Healthc Mater 9:e1901448. https://doi.org/10.1002/adhm.201901448
14. Mariam J, Sivakami S, Dongre PM (2016) Albumin corona on nanoparticles - a strategic approach in drug delivery. Drug Deliv 23:2668–2676. https://doi.org/10.3109/10717544.2015.1048488
15. Sasidharan A, Riviere JE, Monteiro-Riviere NA (2015) Gold and silver nanoparticle interactions with human proteins: impact and implications in biocorona formation. J Mater Chem B Mater Biol Med 3:2075–2082. https://doi.org/10.1039/c4tb01926a
16. Karmali PP, Simberg D (2011) Interactions of nanoparticles with plasma proteins: implication on clearance and toxicity of drug delivery systems. Expert Opin Drug Deliv 8:343–357. https://doi.org/10.1517/17425247.2011.554818
17. Yao T, Asayama Y (2017) Animal-cell culture media: History, characteristics, and current issues. Reprod Med Biol 16:99–117. https://doi.org/10.1002/rmb2.12024
18. Li X, Guo W, Xu R et al (2022) The interaction mechanism between gold nanoparticles and proteins: Lysozyme, trypsin, pepsin, γ-globulin, and hemoglobin. Spectrochim Acta A Mol Biomol Spectrosc 272:120983. https://doi.org/10.1016/j.saa.2022.120983
19. Waghmare M, Khade B, Chaudhari P, Dongre P (2018) Multiple layer formation of bovine serum albumin on silver nanoparticles revealed by dynamic light scattering and spectroscopic techniques. J Nanopart Res 20:185. https://doi.org/10.1007/s11051-018-4286-3
20. Zolghadri S, Saboury AA, Golestani A et al (2009) Interaction between silver nanoparticle and bovine hemoglobin at different temperatures. J Nanopart Res 11:1751–1758. https://doi.org/10.1007/s11051-008-9538-1
21. Hansen U, Thünemann AF (2015) Characterization of silver nanoparticles in cell culture medium containing fetal bovine serum. Langmuir 31:6842–6852. https://doi.org/10.1021/acs.langmuir.5b00687
22. Poulsen KM, Payne CK (2022) Concentration and composition of the protein corona as a function of incubation time and serum concentration: an automated approach to the protein corona. Anal Bioanal Chem 414:7265–7275. https://doi.org/10.1007/s00216-022-04278-y
23. Gun'ko VM, Mikhalovska LI, Tomlins PE, Mikhalovsky SV, (2011) Competitive adsorption of macromolecules and real-time dynamics of Vroman-like effects. Phys Chem Chem Phys 13:4476–4485. https://doi.org/10.1039/c0cp02165b
24. Chakraborty D, Ethiraj KR, Mukherjee A (2020) Understanding the relevance of protein corona in nanoparticle-based therapeutics and diagnostics. RSC Adv 10:27161–27172. https://doi.org/10.1039/d0ra05241h
25. Digiacomo L, Pozzi D, Palchetti S et al (2020) Impact of the protein corona on nanomaterial immune response and targeting ability. Wiley Interdiscip Rev Nanomed Nanobiotechnol 12:e1615. https://doi.org/10.1002/wnan.1615
26. Maiorano G, Sabella S, Sorce B et al (2010) Effects of cell culture media on the dynamic formation of protein-nanoparticle complexes and influence on the cellular response. ACS Nano 4:7481–7491. https://doi.org/10.1021/nn101557e
27. Turkevich J, Stevenson PC, Hillier J (1951) A study of the nucleation and growth processes in the synthesis of colloidal gold. Discuss Faraday Soc 11:55. https://doi.org/10.1039/df9511100055
28. Glatter O (1977) A new method for the evaluation of small-angle scattering data. J Appl Crystallogr 10:415–421. https://doi.org/10.1107/S0021889877013879
29. Oliveira CLP, Behrens MA, Pedersen JS et al (2009) A SAXS study of glucagon fibrillation. J Mol Biol 387:147–161. https://doi.org/10.1016/j.jmb.2009.01.020
30. Oliveira CLP (2011) Investigating macromolecular complexes in solution by small angle X-ray scattering. Current Trends in X-Ray Crystallography. https://doi.org/10.5772/30730
31. Vignoli Muniz GS, Souza MC, Duarte EL, Lamy MT (2021) Comparing the interaction of the antibiotic levofloxacin with zwitterionic and anionic membranes: Calorimetry, fluorescence, and spin label studies. Biochim Biophys Acta Biomembr 1863:183622. https://doi.org/10.1016/j.bbamem.2021.183622
32. Zhang X-F, Liu Z-G, Shen W, Gurunathan S (2016) Silver nanoparticles: synthesis, characterization, properties, applications, and therapeutic approaches. Int J Mol Sci 17. https://doi.org/10.3390/ijms17091534
33. Precupas A, Ruxandra Leonties A, Neacsu A et al (2022) Bovine hemoglobin thermal stability in the presence of naringenin: Calorimetric, spectroscopic and molecular modeling studies. J Mol Liq 361:119617. https://doi.org/10.1016/j.molliq.2022.119617
34. Dąbkowska M, Kosiorowska A, Machaliński B (2023) The impact of serum protein adsorption on PEGylated NT3-BDNF nanoparticles-distribution, protein release, and cytotoxicity in a human retinal pigmented epithelial cell model. Pharmaceutics 15. https://doi.org/10.3390/pharmaceutics15092236
35. Gunnarsson SB, Bernfur K, Englund-Johansson U et al (2019) Analysis of complexes formed by small gold nanoparticles in low concentration in cell culture media. PLoS ONE 14:e0218211. https://doi.org/10.1371/journal.pone.0218211
36. Li X, Wang X, Liu H et al (2021) Mechanism evaluation of the interactions between eight flavonoids and γ-globulin based on multi-spectroscopy. J Mol Struct 1225:129291. https://doi.org/10.1016/j.molstruc.2020.129291
37. Bhomia R, Trivedi V, Coleman NJ, Mitchell JC (2016) The thermal and storage stability of bovine haemoglobin by ultraviolet-visible and circular dichroism spectroscopies. J Pharm Anal 6:242–248. https://doi.org/10.1016/j.jpha.2016.02.004
38. Li Z, Shen W, Liu X, Liu R (2017) Efficient unimolecular photoinitiators for simultaneous hybrid thiol–yne–epoxy photopolymerization under visible LED light irradiation. Polym Chem 8:1579–1588. https://doi.org/10.1039/C7PY00159B
39. Perera YR, Xu JX, Amarasekara DL et al (2021) Understanding the adsorption of peptides and proteins onto PEGylated gold nanoparticles. Molecules 26. https://doi.org/10.3390/molecules26195788

40. Bhattacharjee S (2016) DLS and zeta potential - What they are and what they are not? J Control Release 235:337–351. https://doi.org/10.1016/j.jconrel.2016.06.017
41. Montes Ruiz-Cabello FJ, Trefalt G, Maroni P, Borkovec M (2014) Electric double-layer potentials and surface regulation properties measured by colloidal-probe atomic force microscopy. Phys Rev E Stat Nonlin Soft Matter Phys 90:012301. https://doi.org/10.1103/PhysRevE.90.012301
42. Li B, Ryan PW, Shanahan M et al (2011) Fluorescence excitation-emission matrix (EEM) spectroscopy for rapid identification and quality evaluation of cell culture media components. Appl Spectrosc 65:1240–1249. https://doi.org/10.1366/11-06383
43. Sharma A, Sarmah S, Roy AS, Ghosh KS (2022) Multispectroscopic studies on the molecular interactions between bovine γ-globulin and borohydride-capped silver nanoparticles. Luminescence 37:1200–1207. https://doi.org/10.1002/bio.4276
44. Stolnik S, Illum L, Davis SS (1995) Long circulating microparticulate drug carriers. Adv Drug Deliv Rev 16:195–214. https://doi.org/10.1016/0169-409X(95)00025-3
45. Huang K, Hu Y, Yu C et al (2016) Charged surface groups of nanoparticles and the adsorbed proteins codetermine the fate of nanoparticles upon interacting with cells. RSC Adv 6:58315–58324. https://doi.org/10.1039/C6RA07468E
46. Yue Z-G, Wei W, Lv P-P et al (2011) Surface charge affects cellular uptake and intracellular trafficking of chitosan-based nanoparticles. Biomacromol 12:2440–2446. https://doi.org/10.1021/bm101482r
47. Stebounova LV, Guio E, Grassian VH (2011) Silver nanoparticles in simulated biological media: a study of aggregation, sedimentation, and dissolution. J Nanopart Res 13:233–244. https://doi.org/10.1007/s11051-010-0022-3
48. Marucco A, Aldieri E, Leinardi R et al (2019) Applicability and limitations in the characterization of poly-dispersed engineered nanomaterials in cell media by dynamic light scattering (DLS). Materials (Basel) 12. https://doi.org/10.3390/ma12233833
49. Han X, Corson N, Wade-Mercer P et al (2012) Assessing the relevance of in vitro studies in nanotoxicology by examining correlations between in vitro and in vivo data. Toxicology 297:1–9. https://doi.org/10.1016/j.tox.2012.03.006
50. González-García LE, MacGregor MN, Visalakshan RM et al (2022) Nanoparticles surface chemistry influence on protein corona composition and inflammatory responses. Nanomaterials (Basel) 12. https://doi.org/10.3390/nano12040682
51. Marucco A, Catalano F, Fenoglio I et al (2015) Possible chemical source of discrepancy between in vitro and in vivo tests in nanotoxicology caused by strong adsorption of buffer components. Chem Res Toxicol 28:87–91. https://doi.org/10.1021/tx500366a
52. Li T, Senesi AJ, Lee B (2016) Small angle x-ray scattering for nanoparticle research. Chem Rev 116:11128–11180. https://doi.org/10.1021/acs.chemrev.5b00690
53. Almatroudi A (2020) Silver nanoparticles: synthesis, characterisation and biomedical applications. Open Life Sci 15:819–839. https://doi.org/10.1515/biol-2020-0094
54. Florin E, Kjellander R, Eriksson JC (1984) Salt effects on the cloud point of the poly(ethylene oxide)+ water system. J Chem Soc, Faraday Trans 1(80):2889. https://doi.org/10.1039/f19848002889
55. Reshetnyak YK, Burstein EA (2001) Decomposition of protein tryptophan fluorescence spectra into log-normal components. II. The statistical proof of discreteness of tryptophan classes in proteins. Biophys J 81:1710–1734. https://doi.org/10.1016/S0006-3495(01)75824-9
56. Lakowicz JR (1983) Quenching of Fluorescence. Principles of fluorescence spectroscopy. Springer, US, Boston, MA, pp 257–301
57. Lewis DJ, Day TM, MacPherson JV, Pikramenou Z (2006) Luminescent nanobeads: attachment of surface reactive Eu(III) complexes to gold nanoparticles. Chem Commun 1433–1435. https://doi.org/10.1039/b518091k
58. Santos JJ, Toma SH, Corio P, Araki K (2017) Key role of surface concentration on reproducibility and optimization of SERS sensitivity. J Raman Spectrosc 48:1190–1195. https://doi.org/10.1002/jrs.5203
59. Silveira RL, Mamián-López MB, Rubim JC et al (2019) Spectroscopic and electrophoresis study of substitution on the surface of gold nanoparticles by different mercaptoalkyl carboxylic acids and bioconjugation with bovine serum albumin. Anal Bioanal Chem 411:3047–3058. https://doi.org/10.1007/s00216-019-01758-6
60. Wang G, Liu X, Yan C et al (2015) Probing the binding of trypsin to glutathione-stabilized gold nanoparticles in aqueous solution. Colloids Surf B Biointerfaces 135:261–266. https://doi.org/10.1016/j.colsurfb.2015.07.063
61. Kopac T (2021) Protein corona, understanding the nanoparticle-protein interactions and future perspectives: A critical review. Int J Biol Macromol 169:290–301. https://doi.org/10.1016/j.ijbiomac.2020.12.108
62. Ross PD, Subramanian S (1981) Thermodynamics of protein association reactions: forces contributing to stability. Biochemistry 20:3096–3102. https://doi.org/10.1021/bi00514a017
63. Nguyen DD, Lue SJ, Lai J-Y (2021) Tailoring therapeutic properties of silver nanoparticles for effective bacterial keratitis treatment. Colloids Surf B Biointerfaces 205:111856. https://doi.org/10.1016/j.colsurfb.2021.111856
64. Cui T, Ma Y, Yang J-Y et al (2021) Protein corona-guided tumor targeting therapy via the surface modulation of low molecular weight PEG. Nanoscale 13:5883–5891. https://doi.org/10.1039/d1nr00426c
65. Park MVDZ, Neigh AM, Vermeulen JP et al (2011) The effect of particle size on the cytotoxicity, inflammation, developmental toxicity and genotoxicity of silver nanoparticles. Biomaterials 32:9810–9817. https://doi.org/10.1016/j.biomaterials.2011.08.085